

Bjorken polarized sum rule and infrared-safe QCD couplings

César Ayala¹, Gorazd Cvetič^{1,a} , Anatoly V. Kotikov², Binur G. Shaikhatdenov²

¹ Department of Physics, Universidad Técnica Federico Santa María (UTFSM), Casilla 110-V, Valparaíso, Chile

² Joint Institute for Nuclear Research, 141980 Dubna, Russia

Received: 25 July 2018 / Accepted: 2 December 2018 / Published online: 10 December 2018
© The Author(s) 2018

Abstract Experimental data obtained for the polarized Bjorken sum rule (BSR) $\Gamma_1^{p-n}(Q^2)$ are fitted by using predictions derived within a truncated operator product expansion (OPE) approach to QCD. Four QCD versions are considered: perturbative QCD (pQCD) in the $\overline{\text{MS}}$ scheme, Analytic Perturbation Theory (APT), and 2δ and 3δ analytic QCD versions. In contrast to pQCD, these QCD variants do not have Landau singularities at low positive Q^2 , which facilitates the fitting procedure significantly. The fitting procedure is applied first to the experimental data of the inelastic part of BSR, and the known elastic contributions are added after the fitting. In general, when 2δ and 3δ QCD coupling is used the fitted curves give the best results, within the Q^2 -range of the fit as well as in extended Q^2 -intervals. When the fitting procedure is applied to the total BSR, i.e., to the sum of the experimental data and the elastic contribution, the quality of the results deteriorates significantly.

1 Introduction

The polarized Bjorken sum rule (BSR) $\Gamma_1^{p-n}(Q^2)$ [1, 2] is an important spacelike QCD observable for various reasons. It is a difference of the first moment of the spin-dependent structure functions of proton and neutron, therefore its isovector nature makes it easier to describe it theoretically, in pQCD in terms of OPE, than the separate integrals of the two nucleons. Further, high quality experimental results for this quantity, obtained in polarized deep inelastic scattering (DIS), are now available in a large range of spacelike squared momenta $-q^2 \equiv Q^2: 0.054 \text{ GeV}^2 \leq Q^2 < 5 \text{ GeV}^2$ [3–11]. In particular, the newer experimental results [5] with highly reduced statistical uncertainties, extracted mainly from the Jefferson Lab CLAS EG1-DVCS experiment [12] taken on polarized targets made of protons and deuterons, render BSR an attrac-

tive quantity to test on it various extensions of pQCD to low $Q^2 \lesssim 1 \text{ GeV}^2$.

Theoretically, pQCD (with OPE), in $\overline{\text{MS}}$ scheme, has been the usual approach to describe such quantities, cf. [3–5]. This approach, however, has the theoretical disadvantage that the running coupling $a(Q^2) [\equiv \alpha_s(Q^2)/\pi]$ possesses Landau singularities at low positive $Q^2 \lesssim 0.1 \text{ GeV}^2$, and this makes it inconvenient for evaluation of spacelike observables $\mathcal{D}(Q^2)$ at low Q^2 , such as BSR. In recent years, an extension of pQCD couplings to low Q^2 , without Landau singularities, called (Fractional) Analytic Perturbation Theory [(F)APT] [13–27] has been applied in the fitting of the theoretical OPE expression to the experimental inelastic contributions to BSR [28–31], with good results.

In this work we fit the theoretical OPE expressions to the experimental BSR results in pQCD, in (F)APT, and two additional extensions of QCD to low Q^2 , namely the 2δ [32, 33] and 3δ [34, 35] \mathcal{A} QCD. The latter two extensions have the coupling $\mathcal{A}(Q^2)$ [the analog of the pQCD coupling $a(Q^2)$] which is free of Landau singularities and physically motivated in the entire relevant regime of Q^2 in the complex plane, $Q^2 \in \mathbb{C} \setminus (-\infty, -M_{\text{thr}}^2]$, where $M_{\text{thr}}^2 \lesssim 1 \text{ GeV}^2$ is a positive threshold scale. The present work is an extension of our previous work on BSR [36, 37]; in comparison with the latter work, we now vary the Q^2 -range of the fit, include the consideration of the elastic contribution, and estimate the uncertainties of the values of the extracted fit parameters due to systematic (in addition to statistical) uncertainties of the experimental BSR data.

The mentioned QCD variants (F)APT, 2δ and 3δ \mathcal{A} QCD were constructed directly by imposing certain physically motivated conditions on the QCD coupling. In this context, we point out that there exist several other approaches to the construction of the QCD coupling, among them those using Dyson–Schwinger equations which involve various versions of the dynamically generated gluon mass (the mentioned 2δ \mathcal{A} QCD gives a coupling with similar properties). For a recent review of various approaches, we refer to [38].

^a e-mail: Gorazd.Cvetic@usm.cl

In Sect. 2 we present the theoretical leading-twist and higher-twist OPE contributions for the considered quantity BSR, as well as the parametrization of the elastic contribution to BSR. In Sect. 3 we present the results of various fits of theoretical expressions to the experimental results. Finally, in Sect. 4 we summarize our conclusions.

Most of the formal aspects of the calculations are relegated to Appendices: in Appendix A we present the form of the leading-twist perturbation coefficients for a general renormalization scale and scheme; in Appendix B we present construction of \mathcal{A}_n , the analogs of pQCD powers a^n , in extensions of pQCD without Landau singularities; in Appendix C we summarize such extensions [(F)APT, 2δ and 3δ]; in Appendix D we explain how the statistical and systematic uncertainties of the experimental data are reflected in the corresponding uncertainties of the parameters extracted in the fits; and in Appendix E we estimate the effects of the finiteness of the charm quark mass in our evaluations.

2 Bjorken sum rule: theoretical expressions

The polarized Bjorken sum rule (BSR), Γ_1^{p-n} , is defined as the difference between proton and neutron polarized structure functions g_1 integrated over the whole x -Bjorken interval

$$\Gamma_1^{p-n}(Q^2) = \int_0^1 dx \left[g_1^p(x, Q^2) - g_1^n(x, Q^2) \right]. \tag{1}$$

Based on the various measurements of these and the related structure functions, the inelastic part of the above quantity, $\Gamma_1^{p-n}(Q^2)_{\text{inel.}}$, has been extracted at various values of squared momenta Q_j^2 ($0.054 \text{ GeV}^2 \leq Q_j^2 < 5 \text{ GeV}^2$): [3–5] (Jefferson Lab), [8, 9] (SLAC), [6, 7] (COMPASS at CERN).¹

Theoretically, this quantity can be written in the Operator Product Expansion (OPE) form [1, 2]

$$\Gamma_1^{p-n, \text{OPE}}(Q^2) = \left| \frac{g_A}{g_V} \right| \frac{1}{6} (1 - \mathcal{D}_{\text{BS}}(Q^2)) + \sum_{i=2}^{\infty} \frac{\mu_{2i}(Q^2)}{Q^{2i-2}}. \tag{2}$$

Here, $|g_A/g_V|$ is the ratio of the nucleon axial charge, $(1 - \mathcal{D}_{\text{BS}})$ is the perturbation expansion for the leading-twist contribution, and μ_{2i}/Q^{2i-2} are the higher-twist contributions. The value obtained from neutron β decay is known to a high accuracy, $|g_A/g_V| = 1.2723 \pm 0.0023$ [39], and we will use the central value. In the higher-twist terms, we will take only the terms $\sim 1/Q^2$ and $1/(Q^2)^2$.

¹ The index j in Q_j^2 indicates from here on that these are the scales at which the experimental values are given.

2.1 Perturbation expansion of the leading-twist

The leading-twist term has the canonical part $\mathcal{D}_{\text{BS}}(Q^2)$ whose perturbation expansion in $a \equiv \alpha_s/\pi$ is known up to N³LO ($\sim a^4$)

$$\mathcal{D}_{\text{BS}}(Q^2)_{\text{pt}} = \bar{a} + \bar{d}_1 \bar{a}^2 + \bar{d}_2 \bar{a}^3 + \bar{d}_3 \bar{a}^4 + \mathcal{O}(\bar{a}^5), \tag{3}$$

where the bar indicates that the expansion is in the $\overline{\text{MS}}$ scheme, and the renormalization scale μ^2 is implicitly understood to be equal to the physical scale Q^2 . The NLO, N²LO and N³LO coefficients \bar{d}_j ($j = 1, 2, 3$) were obtained in [40–42], respectively. In the considered range of momentum transfer $0 < Q^2 < 5 \text{ GeV}^2$, we will assume that the effective number of active quark flavors is $N_f = 3$, and therefore only the nonsinglet (NS) contributions appear.²

When the renormalization scale is changed from $\mu^2 = Q^2$ to a general value $\mu^2 = kQ^2$ ($0 < k \sim 1$), and when the renormalization scheme parameters are changed from the $\overline{\text{MS}}$ values $\bar{c}_j \equiv \bar{\beta}_j/\beta_0$ to general scheme parameter values c_j ($j \geq 2$), the perturbation expansion changes accordingly

$$\mathcal{D}_{\text{BS}}(Q^2)_{\text{pt}} = a(kQ^2) + d_1(k)a(kQ^2)^2 + d_2(k; c_2)a(kQ^2)^3 + d_3(k; c_2, c_3)a(kQ^2)^4 + \mathcal{O}(a^5). \tag{4}$$

The expressions for the new coefficients $d_1(k)$, $d_2(k; c_2)$ and $d_3(k; c_2, c_3)$ are obtained on the basis of independence of the observable $\mathcal{D}_{\text{BS}}(Q^2)_{\text{pt}}$ from k and c_j ($j \geq 2$), and are given in Appendix A.

In those versions of $\mathcal{A}\text{QCD}$ where the coupling is a holomorphic function $\mathcal{A}(Q^2)$ [instead of the nonholomorphic $a(Q^2)$] with nonperturbative contributions, the power expansion (4) becomes a nonpower expansion where a^n get replaced by \mathcal{A}_n ($\neq \mathcal{A}^n$)

$$\mathcal{D}_{\text{BS}}(Q^2)_{\mathcal{A}\text{QCD}} = \mathcal{A}(kQ^2) + d_1(k)\mathcal{A}_2(kQ^2) + d_2(k; c_2)\mathcal{A}_3(kQ^2) + d_3(k; c_2, c_3)\mathcal{A}_4(kQ^2) + \mathcal{O}(\mathcal{A}_5). \tag{5}$$

The construction of the power analogs \mathcal{A}_n of a^n were obtained in Ref. [45, 46] for integer n and in Ref. [47] for general real $n > -1$. A brief description for the construction of \mathcal{A}_n is given in Appendix B. These expressions are based on the renormalization group equation (RGE), in close analogy with the RGE in the perturbation theory. The couplings $\mathcal{A}_n(Q^2)$ can be obtained once the coupling $\mathcal{A}(Q^2)$ is known. The construction of $\mathcal{A}(Q^2)$ coupling is summarized in Appendix C for various variants of QCD with holomorphic coupling: (F)APT, 2δ and 3δ $\mathcal{A}\text{QCD}$, and we refer to that Appendix for more details.

² The singlet contribution appears for the first time at $\sim a^4$, and only if $N_f \neq 3$ [43, 44].

2.2 Higher-twist

In the theoretical OPE expression (2), the term with the dimension $D = 2$ (i.e., $\propto 1/Q^2$) has the coefficient

$$\mu_4 = \frac{M_N^2}{9}(a_2^{p-n} + 4d_2^{p-n} + 4f_2^{p-n}(Q^2)), \tag{6}$$

where $M_N \approx 0.94$ GeV is the nucleon mass, a_2^{p-n} is the (twist-2) target mass correction, and d_2^{p-n} is a twist-3 matrix element

$$d_2^{p-n} = \int_0^1 dx x^2 (2g_1^{p-n} + 3g_2^{p-n}). \tag{7}$$

At $Q^2 = 1$ GeV², we have $a_2^{p-n} = 0.031 \pm 0.010$ and $d_2^{p-n} = 0.008 \pm 0.0036$ [5]. We will neglect Q^2 -dependence of these two quantities [as was done also in Ref. [5]], and will take the central values, i.e., $a_2^{p-n} + 4d_2^{p-n} = 0.063$. On the other hand, the coefficient $f_2^{p-n}(Q^2)$ will be a parameter of the fit, and its Q^2 -dependence will not be neglected, its evolution is known [48, 49] in pQCD

$$f_2^{p-n}(Q^2) = f_2^{p-n}(Q_{in}^2) \left(\frac{a(Q^2)}{a(Q_{in}^2)} \right)^{\gamma_0/8\beta_0}, \tag{8}$$

where $\nu \equiv \gamma_0/(8\beta_0) = 32/81$ when $N_f = 3$, and the reference scale will be taken $Q_{in}^2 = 1$ GeV². In QCD with holomorphic coupling $\mathcal{A}(Q^2)$, the power $a^{\gamma_0/8\beta_0}$ gets replaced by $\mathcal{A}_{\gamma_0/8\beta_0}$ (which is in general not equal to the simple power $\mathcal{A}^{\gamma_0/8\beta_0}$, as mentioned above, cf. also Appendix B,

$$f_2^{p-n}(Q^2) = f_2^{p-n}(Q_{in}^2) \left(\frac{\mathcal{A}_{\gamma_0/8\beta_0}(Q^2)}{\mathcal{A}_{\gamma_0/8\beta_0}(Q_{in}^2)} \right), \tag{9}$$

In addition, in some of the fits we will also include the $D = 4$ term in the theoretical OPE expression (2) $\mu_6/(Q^2)^2$, where we will consider the coefficient μ_6 as Q^2 -independent. Thus, our theoretical expression for BSR will be the truncated (at $D = 4$, or $D = 2$) OPE expression

$$\Gamma_1^{p-n, \text{OPE}[4]}(Q^2; k, f_2^{p-n}(1); \mu_6) = \left| \frac{g_A}{g_V} \right| \frac{1}{6} (1 - \mathcal{D}_{BS}(Q^2)) + \frac{M_N^2}{Q^2} \frac{1}{9} (a_2^{p-n} + 4d_2^{p-n} + 4f_2^{p-n}(Q^2)) + \frac{\mu_6}{(Q^2)^2}, \tag{10}$$

where the leading-twist truncated expressions are given in Eqs. (4) and (5), and the Q^2 -dependent part of the $D = 2$ term (twist-4) in Eqs. (8) and (9), for the pQCD and AQCD version of QCD, respectively. We will regard the renormalization scale parameter $k \equiv \mu^2/Q^2$ and the higher-twist coefficients $f_2^{p-n}(Q_{in}^2)$ (with $Q_{in}^2 = 1$ GeV²) and μ_6 as the free parameters to be determined in the fitting procedure.

In our approach, we will include in the leading-twist part of the OPE all the known terms (i.e., up to order $\sim a^4 \sim \mathcal{A}_4$). The order of the leading-twist terms in general affects the

fitted higher-twist contributions (cf. [50–57] for the fit of truncated OPE to structure functions).

2.3 Elastic contribution

The OPE evaluation is, in principle, for inclusive observables; in the case of BSR, this means that the OPE fit should be applied to the experimental values of the sum of the inelastic and elastic contribution.

The elastic contribution to BSR can be expressed [58, 59] in terms of the proton and neutron electromagnetic form factors F_1 and F_2

$$\Gamma_1^{p-n}(Q^2)_{\text{el.}} = \frac{1}{2} F_1^p(Q^2) (F_1^p(Q^2) + F_2^p(Q^2)) - \frac{1}{2} F_1^n(Q^2) (F_1^n(Q^2) + F_2^n(Q^2)). \tag{11}$$

The most recent parametrization of these form factors was performed in [60] from light-front holographic QCD (LFH QCD). Namely, these form factors can be expressed in terms of the inverse power expressions

$$\mathcal{F}_\tau \equiv \left(1 + \frac{Q^2}{M_\rho^2} \right)^{-1} \times \dots \times \left(1 + \frac{Q^2}{(2\tau - 3)M_\rho^2} \right)^{-1}, \tag{12}$$

$(\tau = 2, 3, \dots),$

which are products of $\tau - 1$ poles along the vector meson Regge radial trajectory in terms of the ρ -vector mass $M_\rho = 0.755$ GeV and its radial excitations. We have

$$F_1^p(Q^2) = \mathcal{F}_{\tau=3}(Q^2),$$

$$F_2^p(Q^2) = \chi_p \left[(1 - \gamma_p) \mathcal{F}_{\tau=4}(Q^2) + \gamma_p \mathcal{F}_{\tau=6}(Q^2) \right], \tag{13a}$$

$$F_1^n(Q^2) = -\frac{1}{3} r \left[\mathcal{F}_{\tau=3}(Q^2) - \mathcal{F}_{\tau=4}(Q^2) \right],$$

$$F_2^n(Q^2) = \chi_n \left[(1 - \gamma_n) \mathcal{F}_{\tau=4}(Q^2) + \gamma_n \mathcal{F}_{\tau=6}(Q^2) \right]. \tag{13b}$$

Here: $\chi_p = \mu_p - 1 = 1.793$ and $\chi_n = \mu_n = -1.913$ are the anomalous moments of p and n , respectively; $\gamma_{n,p}$ are the higher Fock probabilities for the $L = 0 \rightarrow L = 1$ spin-flip electromagnetic form factors, and r is a phenomenological factor. The values of these three parameters are obtained by fitting to polarization data for the form factors [60]: $\gamma_p = 0.27$; $\gamma_n = 0.38$; $r = 2.08$.

As a consequence, the elastic contribution (11) can be represented as a combination of inverse powers $(1 + Q^2/M_\rho^2/(2m - 1))$, and for large Q^2 this can be expanded in inverse powers of Q^2

$$\Gamma_1^{p-n}(Q^2)_{\text{el.}} = 2.3368 \left(\frac{M_\rho^2}{Q^2} \right)^4 + 13.8851 \left(\frac{M_\rho^2}{Q^2} \right)^5 + \mathcal{O}(1/Q^{12}). \quad (14)$$

This means that at high Q^2 the elastic contribution starts with the dimension $D = 8$ term $\sim (1/Q^2)^4$. Theoretically, it is not included in the truncated OPE expression (10) in pQCD.^{3,4} Further, in 3δ and 2δ AQCD, the higher dimensional terms up to (and including) the $D = 8$ term are not included in the leading-twist contribution (5) because in these approaches $\mathcal{A}(Q^2) - a(Q^2) \sim (\Lambda^2/Q^2)^5$ as explained in Appendix C.2 Eq. (C7). Therefore, the truncated OPE expression (10) does not contain the dimension $D = 8$ term $\sim (1/Q^2)^4$ also in 3δ and 2δ AQCD approaches. The only exception is the (F)APT where $\mathcal{A}(Q^2) - a(Q^2) \sim (\Lambda^2/Q^2)^1$, cf. Appendix C.1, and where the truncated OPE (10) could contain, in principle, all the elastic contributions, including the $\sim (1/Q^2)^4$ term.

Therefore, it looks more natural to first fit the truncated OPE expression (10), with pQCD and (3δ and 2δ) AQCD, to the BSR experimental results [3–5, 7, 8] which are obtained for the inelastic contribution; and after such a fit, add the elastic contribution (11) [with the parametrization (12)–(13b)]. We note that the theoretical expression obtained for the total BSR in this way is the sum of the expressions (10) and (11), which is again an OPE expression as it should be for such an inclusive spacelike observable as the total BSR.

The other approach would be to fit the truncated OPE expression (10) with the experimental points for the total BSR, i.e., fit with the experimental points for inelastic BSR with the elastic contribution added to them. Such an approach seems less natural, at least in pQCD and 3δ and 2δ AQCD, because the truncated expression (10) in these cases in principle does not contain the leading elastic contribution $\sim 1/(Q^2)^4$, cf. Eq. (C7) in Appendix C.2.

Nonetheless, below we will apply, for completeness, both approaches in our numerical fitting procedures.

³ However, the last coefficient in the truncated OPE, e.g. μ_6 , is sometimes in the literature regarded to include, in a certain effective way, the contributions from the higher dimensional terms $D \geq 6$, cf. [5] for a discussion of these aspects.

⁴ The elastic contributions parametrized in a way different from that of Ref. [60] could in general contain terms of dimension $D < 8$. Nonetheless, the fitted expressions of Ref. [59] give for the elastic contributions an expansion similar to Eq. (14), where the first nonzero term is a very small $D = 6$ contribution which is negligible in comparison with $D = 8$ term (the coefficient at $D = 6$ term is by about a factor of 10^{-4} smaller than at $D = 8$ term). All these terms there are divided by a large weakly Q^2 -dependent factor $[\ln(27.81 + 1.72 Q^2/M_\rho^2)]^{4.296}$.

3 Numerical fits

In the numerical fits, we will consider the following parameters to be fitted in the truncated OPE expression (10): (i) the renormalization scale parameter $k \equiv \mu^2/Q^2$ of the (truncated) leading-twist contribution (4) [for pQCD] or (5) [for AQCD]; (ii) the parameter $f_2^{p-n}(1 \text{ GeV}^2)$ appearing in the $D = 2$ term of Eq. (10) [cf. Eqs. (8) and (9)]; (iii) and in some fits the parameter μ_6 in the $D = 4$ term of Eq. (10) will be included. We will take for the experimental data points for the inelastic contribution to BSR the data from [3–5, 7, 8];⁵ they are in the momentum interval $0.054 \text{ GeV}^2 \leq Q_j^2 < 5 \text{ GeV}^2$. Among these data points, we exclude from the fit the four points with $Q_j^2 \geq 3 \text{ GeV}^2$ (three from [5], at $Q_j^2 = 3.223, 3.871$ and 4.739 GeV^2 ; and one from [7] at $Q^2 = 3 \text{ GeV}^2$) because they tend to decrease the quality parameter $\chi^2/(\text{d.o.f.})$ of the fit significantly. Nonetheless, we will show both quality parameters $\chi^2/(\text{d.o.f.})$ obtained from the mentioned fits, i.e., the one with the four points excluded, and included.⁶ The number of active flavors will be kept all the time at $N_f = 3$. The fits will be performed by the least squares method, taking into account the statistical uncertainties $\sigma_{j,\text{stat}}$ in the points Q_j^2 , we will consider them independent of each other. These uncertainties $\sigma_{j,\text{stat}}$ are in general significantly smaller than the systematic uncertainties $\sigma_{j,\text{sys}}$. The latter are strongly correlated, and we will consider them as completely correlated. The uncertainties in the values of the extracted parameters $k \equiv \mu^2/Q^2$, $f_2^{p-n}(Q_{\text{in}}^2)$ and μ_6 are then due to statistical (small) and systematic (larger) uncertainties of the data. We refer to Appendix D on how we obtained the uncertainties of the extracted values of the fit parameters.

Using specific values of the renormalization scale parameter $k \equiv \mu^2/Q^2$ may allow us to incorporate in our evaluations (5) at least a part of the contributions of higher orders of the series. It is expected that $k \sim 1$, and usually it is taken in the literature in the range $1/2 < k < 2$, sometimes $1/4 < k < 4$. In the considered work, after replacing the powers of the pQCD coupling by their analytic counterparts, cf. Eqs. (4)–(5), a spacelike observable depends usually weakly on the contributions of higher orders. Still, in order not to miss the possibly relevant influence of higher orders, we decided to increase the range of possible k values to: $1/16 < k < 16$. This choice still avoids very large or very small renormalization scales where the corresponding coef-

⁵ We will not take into account the SLAC E155, SMC and HERMES points [9–11], at $Q^2 = 5 \text{ GeV}^2, 10 \text{ GeV}^2$, and 2.5 (and 5) GeV^2 , respectively, as they were obtained by NLO pQCD Q^2 -evolution from data distributed across a wide range of Q^2 . Among the points of SLAC E143 we exclude the point at $Q^2 = 5 \text{ GeV}^2$ for the same reason.

⁶ If we perform the fit with the four points included, the results differ somewhat, but not significantly.

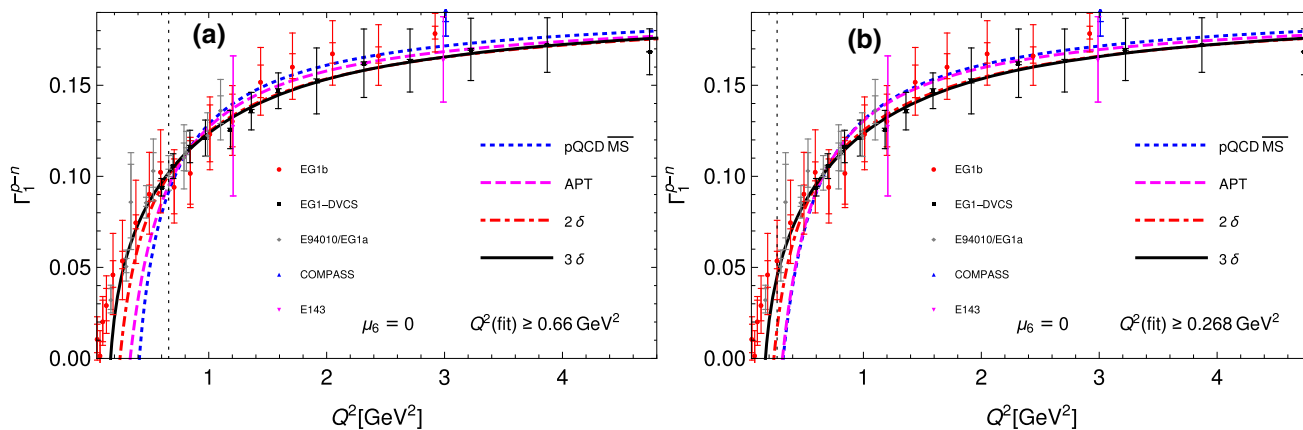


Fig. 1 Fits of the OPE expression (10) truncated at $D = 2$ term, i.e., $\mu_6 = 0$, to the experimental data for $\Gamma_1^{p-n}(Q^2)_{\text{inel.}}$, in four different QCD variants, where in the fits: **a** $Q^2 \geq 0.66 \text{ GeV}^2$; **b**

$Q^2 \geq 0.268 \text{ GeV}^2$. See the text for details. The respective lower bound of the fitting interval, $Q_{\text{min}}^2 = 0.66$ or 0.268 GeV^2 , is included as the thin dotted vertical line

coefficients $d_n(k)$ at the powers $a(kQ^2)^{n+1}$, or at their analytic counterparts $\mathcal{A}_{n+1}(kQ^2)$, contain powers of the large terms $\sim \ln k$ [cf. Eq. (A3)] which may destroy the convergence of the series already at low n . We will see that the results of the fitting will rarely give the extreme values $k = 16$ or $k = 1/16 \approx 0.063$, mostly in the cases of $\overline{\text{MS}}$ pQCD and (F)APT.

We present below the results of the fits of the inelastic contributions to the truncated OPE expression (10), first in Sect. 3.1 with $\mu_6 = 0$, and then in Sect. 3.2 for $\mu_6 \neq 0$ included as a fit parameter; the elastic contribution is added afterwards. In Sect. 3.3 we present the corresponding fits for the case when the higher-twist term in the OPE has a mass parameter. In Sect. 3.4 we include the fits for two different ansätze for BSR at very low Q^2 . Finally, in Sect. 3.5 we present the fits of the truncated OPE expression (10), with $\mu_6 \neq 0$ included as a fit parameter, applied to the total BSR, i.e., to the sum of the inelastic data points (at Q_j^2) and the corresponding elastic contribution $\Gamma_1^{p-n}(Q_j^2)_{\text{el.}}$.

In each case, the fits are performed for four variants of QCD: in pQCD (in $\overline{\text{MS}}$), in (F)APT (in $\overline{\text{MS}}$), and in 2δ [33] and 3δ AQCD [35]. Each of these fits is performed by excluding among the data points those with $Q^2 < Q_{\text{min}}^2$, where $Q_{\text{min}}^2 = 0.268$ or 0.66 GeV^2 (and sometimes also: $Q_{\text{min}}^2 = 0.47 \text{ GeV}^2$). As mentioned earlier, the four points at high $Q^2 \geq 3 \text{ GeV}^2$ are excluded from the fit as well.

It is reasonable to assume that the number of active quark flavors in the considered interval $0.054 \text{ GeV}^2 < Q^2 < 5 \text{ GeV}^2$ is $N_f = 3$, cf. Appendix E. All the fits will be performed in $\overline{\text{MS}}$ pQCD approach, in the Fractional Analytic Perturbation Theory [(F)APT], and in 2δ and 3δ AQCD approach, cf. Appendix C where also the values of the parameters of these three QCD variants are presented. In $\overline{\text{MS}}$ pQCD and in 2δ and 3δ AQCD the (underlying) pQCD

running coupling $a(Q^2)$ is determined by the requirement $\pi a(M_Z^2; \overline{\text{MS}}) = 0.1185$ [39,61], and in (F)APT we use $\overline{\Lambda}_3 = 0.45 \text{ GeV}$ (at the end of Sect. 3.2 we also comment on the case $\overline{\Lambda}_3 = 0.40 \text{ GeV}$); we refer to Appendix C for more details.

3.1 Fits with $\mu_6 = 0$

In Fig. 1a, b, we present the curves in the mentioned four QCD variants, for $Q_{\text{min}}^2 = 0.66$ and 0.268 GeV^2 , respectively. The corresponding results and four fit quality parameters $\chi^2/\text{d.o.f}$ are given in Table 1, for $Q_{\text{min}}^2 = 0.66, 0.47$ and 0.268 GeV^2 . As mentioned earlier, the fit is performed for the data in the momentum interval $Q_{\text{min}}^2 \leq Q_j^2 \leq 3 \text{ GeV}^2$ (with the COMPASS data point [7] excluded), and the corresponding quality parameter for that interval is denoted as $\chi^2/\text{d.o.f}$. In addition, $\chi_{\text{ext}}^2/\text{d.o.f}$. is the quality parameter for the wider interval $Q_{\text{min}}^2 \leq Q_j^2 < 5 \text{ GeV}^2$; $\chi_{0.268}^2/\text{d.o.f}$. is the parameter when $0.268 \text{ GeV}^2 \leq Q_j^2 \leq 3 \text{ GeV}^2$; and $\chi_{\text{all}}^2/\text{d.o.f}$. is the parameter when all the experimental points [3–5,7,8] are included, $0.054 \text{ GeV}^2 \leq Q_j^2 < 5 \text{ GeV}^2$. In these quantities χ^2 , the central values of k and $f_2^{p-n}(Q_{\text{in}}^2)$ ($Q_{\text{in}}^2 = 1 \text{ GeV}^2$) parameters obtained from the mentioned fit interval $Q_{\text{min}}^2 \leq Q_j^2 \leq 3 \text{ GeV}^2$ are used; we take here “d.o.f” as $(N - p)$ where N is the number of fitted data points entering the considered χ^2 and p is the number of parameters of the fit ($p = 2$ here)

$$\begin{aligned} &\chi^2(Q_{k+1}^2 \leq Q^2 \leq Q_{k+N}^2)/\text{d.o.f.} \\ &= \frac{1}{(N-p)} \sum_{j=k+1}^{k+N} \frac{1}{\sigma_{j,\text{stat}}^2} \left(\Gamma_1^{p-n, \text{OPE}[4]}(Q_j^2; k, f_2^{p-n}(1); \mu_6 = 0) \right. \\ &\quad \left. - \Gamma_1^{p-n}(Q_j^2)_{\text{exp}} \right)^2. \end{aligned} \tag{15}$$

Table 1 The values of the extracted fit parameters $k = \mu^2/Q^2$ and $f_2^{p-n}(Q_{\text{in}}^2)$ ($Q_{\text{in}}^2 = 1 \text{ GeV}^2$), obtained by fitting the OPE expression (10), truncated at $D = 2$ ($\mu_6 = 0$), for the considered four QCD variants, and for the minimal Q^2 values of the fit being 0.66, 0.47 and

0.268 GeV^2 . The uncertainties of the extracted f_2^{p-n} values are separated to those coming from the statistical (small) and systematic (large) uncertainties of the experimental data (cf. Appendix D). The resulting fit quality parameters $\chi^2/\text{d.o.f.}$ are given as well (see the text for explanation)

QCD variant	Q_{min}^2 (fit)	k	$f_2^{p-n}(1.)$	$\chi^2/\text{d.o.f.}$	$\chi_{\text{ext}}^2/\text{d.o.f.}$	$\chi_{0.268}^2/\text{d.o.f.}$	$\chi_{\text{all}}^2/\text{d.o.f.}$
$\overline{\text{MS}}$ pQCD	0.66	6.04	$-0.103 \pm 0.001 \pm 0.011$	44.5	161	6.81×10^4	∞
(F)APT	0.66	2.74	$-0.143 \pm 0.001 \pm 0.021$	23.3	85.6	63.0	970
2δ	0.66	0.397	$-0.077 \pm 0.001 \pm 0.024$	8.34	52.2	11.1	406
3δ	0.66	2.41	$-0.064 \pm 0.001 \pm 0.023$	6.85	56.1	6.17	130
$\overline{\text{MS}}$ pQCD	0.47	6.35	$-0.094 \pm 0.000 \pm 0.009$	66.1	177	5.71×10^4	∞
(F)APT	0.47	3.03	$-0.137 \pm 0.000 \pm 0.015$	30.5	88.4	51.2	873
2δ	0.47	0.395	$-0.077 \pm 0.000 \pm 0.023$	7.91	45.2	10.9	402
3δ	0.47	2.58	$-0.064 \pm 0.000 \pm 0.023$	6.49	50.2	5.92	129
$\overline{\text{MS}}$ pQCD	0.268	16	$-0.160 \pm 0.001 \pm 0.045$	58.7	145	58.7	1.20×10^3
(F)APT	0.268	3.71	$-0.134 \pm 0.000 \pm 0.102$	49.6	103	49.6	827
2δ	0.268	0.338	$-0.074 \pm 0.000 \pm 0.022$	10.6	46.6	10.6	372
3δ	0.268	2.55	$-0.064 \pm 0.000 \pm 0.018$	5.91	44.5	5.91	129

The values of these quantities are always large, in the best cases between 1 and 10. This is so because the statistical uncertainties of the newer JLAB data [5] are very small, $\sigma_{j,\text{stat}} \lesssim 10^{-3}$, and simultaneously, our fit function (truncated OPE) is different from the ideal function which we do not know. Nonetheless, they decrease when analytic QCD variants are employed, especially 2δ and 3δ AQCD.

We wish to point out that the approach of $\overline{\text{MS}}$ QCD in the case of $Q_{\text{min}}^2 = 0.268 \text{ GeV}^2$ is, in principle, not applicable. This is so because the corresponding coupling $a(Q^2)$ has a Landau branching point at $Q_{\text{branch}}^2 = 0.371 \text{ GeV}^2$, which makes the $D = 2$ running coefficient $f_2^{p-n}(Q^2)$, Eq. (8), undefined at $Q^2 \leq 0.371 \text{ GeV}^2$. Nonetheless, in order to be able to present a curve, we applied in the fitting case $Q_{\text{min}}^2 = 0.268 \text{ GeV}^2$ in the $\overline{\text{MS}}$ pQCD approach a restriction on the leading-twist renormalization scale $\mu^2 = kQ^2$, namely $k > 1.383$; and this not just in the leading-twist contribution, but we also made an ad hoc replacement in the $D = 2$ running coefficient $f_2^{p-n}(Q^2)$, Eq. (8): $f_2^{p-n}(Q^2) \mapsto f_2^{p-n}(kQ^2)$. We applied this also in the case when $\mu_6 \neq 0$ (Sect. 3.2, for $\overline{\text{MS}}$ pQCD approach with $Q_{\text{min}}^2 = 0.268 \text{ GeV}^2$). In other approaches (APT and AQCD's) this is not necessary, as there are no Landau singularities. Further, we note that in the last column in Table 1 we have $\chi^2/\text{d.o.f.} = \infty$ in the case of $\overline{\text{MS}}$ pQCD for $Q_{\text{min}}^2 = 0.66$ and 0.47 GeV^2 . This is so because at the lowest available experimental point, $Q_{j=1}^2 = 0.054 \text{ GeV}^2$, the coupling is $a(kQ_1^2; \overline{\text{MS}}) = \infty$ because $kQ_1^2 < Q_{\text{branch}}^2 = 0.371 \text{ GeV}^2$ and thus we hit Landau singularities there.

We can deduce from Fig. 1 and Table 1: (a) the best results in the considered approach ($\mu_6 = 0$) are obtained in 3δ

AQCD; (b) the quality of extrapolation of the obtained fitted curves from the fitting interval, $Q_{\text{min}}^2 \leq Q^2 \leq 3 \text{ GeV}^2$, to the entire interval, $0.054 \text{ GeV}^2 \leq Q^2 < 5 \text{ GeV}^2$, does not improve significantly when the fitted interval is extended (i.e., when Q_{min}^2 is lowered), cf. also the last column in Table 1. This indicates that the behavior of the curves in the extrapolated regions, $0.054 \text{ GeV}^2 < Q^2 < 0.268 \text{ GeV}^2$ and $3 \text{ GeV}^2 < Q^2 \leq 5 \text{ GeV}^2$, is of similar quality in the cases of different values of Q_{min}^2 (fit), and gives the dominant part of $\chi_{\text{all}}^2/\text{d.o.f.}$. The same can be observed for the values of $f_2^{p-n}(1)$: they do not depend much on the value of Q_{min}^2 (fit), but only on the QCD variant used in the fit. This appears to be related with the fact that only one parameter beyond the leading-twist contribution is used here ($\mu_4 \leftrightarrow f_2^{p-n}$), representing a truncated OPE ansatz with a significantly restricted freedom.

3.2 Fits with $\mu_6 \neq 0$

When we include μ_6 in the fit as the third parameter, the resulting curves are presented in Fig. 2a, b, for $Q_{\text{min}}^2 = 0.66$ and 0.47 GeV^2 , respectively. Further, when $Q_{\text{min}}^2 = 0.268 \text{ GeV}^2$, the results are shown in Fig. 3a, b, at the higher Q^2 and the lower $Q^2 < 1 \text{ GeV}^2$ momenta, respectively. The corresponding results are given in Table 2, for $Q_{\text{min}}^2 = 0.66, 0.47$ and 0.268 GeV^2 , with the same notations as in Table 1. The various versions of $\chi^2/\text{d.o.f.}$ are those as explained in the previous Sect. 3.1, except that now in the relation (15) the factor in front of the sum is $1/(N - 3)$ ($p = 3$, d.o.f. is $N - 3$).

Comparing Table 2 and Figs. 2 and 3 with Table 1 and the Fig. 1 of the previous Sect. 3.1 where $\mu_6 = 0$ was kept,

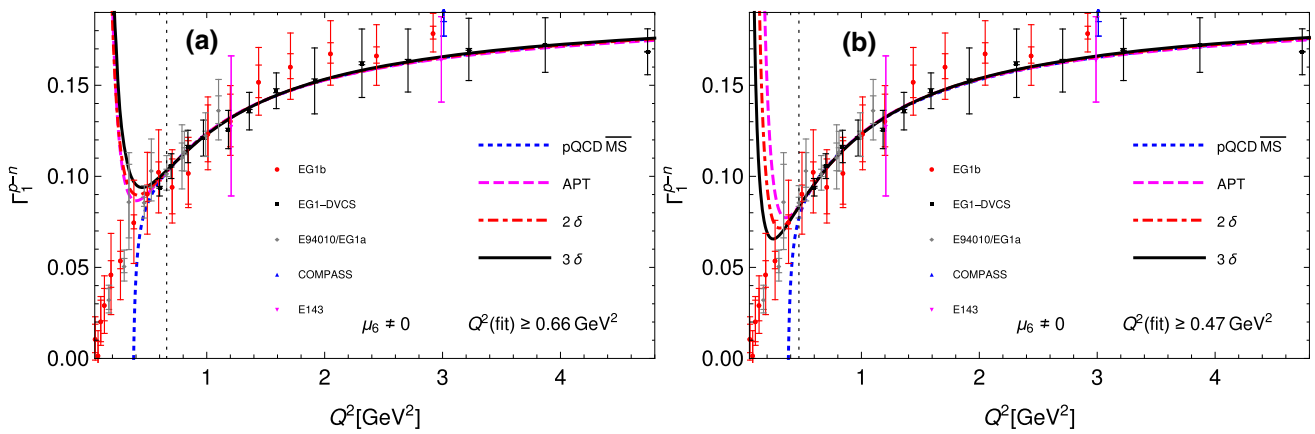


Fig. 2 Fits of the OPE expression (10) truncated at $D = 4$ term (i.e., $\mu_4 \neq 0$), to the experimental data for $\Gamma_1^{p-n}(Q^2)_{\text{incl.}}$, done in four different QCD variants, where in the fits: **a** left plot, $Q^2 \geq 0.66 \text{ GeV}^2$;

b right plot, $Q^2 \geq 0.47 \text{ GeV}^2$. See the text for details. The respective lower bound of the fitting interval, $Q_{\text{min}}^2 = 0.66$ and 0.47 GeV^2 , is included as the thin dotted vertical line

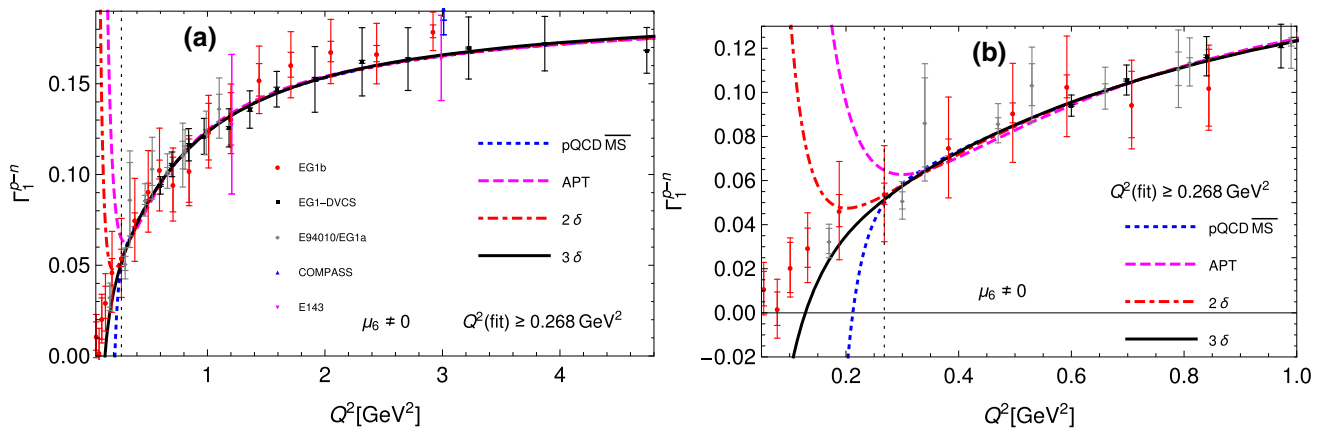


Fig. 3 As Fig. 2, but for $Q_{\text{min}}^2 = 0.268 \text{ GeV}^2$: **a** for larger Q^2 ; **b** for $Q^2 < 1 \text{ GeV}^2$. The lower bound of the fitting interval, $Q_{\text{min}}^2 = 0.268 \text{ GeV}^2$, is included as the thin dotted vertical line

we can see that in the cases of $Q^2(\text{fit}) \geq 0.66 \text{ GeV}^2$ and $Q^2(\text{fit}) \geq 0.47 \text{ GeV}^2$ the $\mu_6 = 0$ fits give in general better $\chi_{\text{all}}^2/\text{d.o.f.}$ (the last columns of Tables 1 and 2). This means that the extrapolation down to the lowest experimental point $Q^2 = Q_{j=1}^2 = 0.054 \text{ GeV}^2$ is better when $\mu_6 = 0$ (with the exception of $\overline{\text{MS}}$ pQCD case where problems with Landau singularities appear). This occurs because the inclusion of the $\mu_6/(Q^2)^2$ term in the truncated OPE makes this expression less stable at very low Q^2 .

On the other hand, when $Q^2(\text{fit}) \geq 0.268 \text{ GeV}^2$, some of the fits (2δ and 3δ AQCD) give better extrapolation when $\mu_6 \neq 0$. Table 2 and Fig. 3 also show that when $\mu_6 \neq 0$ and $Q^2(\text{fit}) \geq 0.268 \text{ GeV}^2$, the best extrapolation to low Q^2 is obtained in 3δ AQCD, followed by 2δ AQCD. As Fig. 3b suggests, the fitted curve in pQCD $\overline{\text{MS}}$ extrapolated to low Q^2 appears to be almost as good; in this case, however, we should keep in mind that the renormalization scale is $\mu^2 = kQ^2$ ($k = 3.00$) and that this scale was used also in $f_2^{p-n}(Q^2)$,

i.e., the ad hoc replacement $f_2^{p-n}(Q^2) \mapsto f_2^{p-n}(kQ^2)$ was performed in order to avoid the Landau singularities in the $D = 2$ term at $Q^2 \geq 0.268 \text{ GeV}^2$ (cf. also the discussion about that point in Sect. 3.1). Despite this replacement, in $\chi_{\text{all}}^2/\text{d.o.f.}$ Landau singularities are hit, because the three lowest experimental points give $kQ_j^2 < Q_{\text{branch}}^2 = 0.371 \text{ GeV}^2$ ($j = 1, 2, 3$) and are thus in the Landau singularity region.⁷

In the case of (F)APT, in contrast to 2δ and 3δ AQCD, the coupling $\mathcal{A}(Q^2)$ differs from the underlying pQCD coupling $a(Q^2)$ nonnegligibly at high $|Q^2| > 1 \text{ GeV}^2$ [the index in Eq. (B1) is $N = 1$ in (F)APT; $N = 5$ in 2δ and 3δ AQCD]. This implies that (F)APT has a certain ambiguity when “normalizing” the strength of $\mathcal{A}(Q^2)$. As mentioned, we fixed the strength of the coupling $\mathcal{A}(Q^2)$ in (F)APT to the value $\overline{\Lambda}_{N_f=3} = 0.45 \text{ GeV}$, since in such a case (F)APT

⁷ We have $Q_1^2 = 0.054 \text{ GeV}^2$, $Q_2^2 = 0.078 \text{ GeV}^2$, and $Q_3^2 = 0.101 \text{ GeV}^2$.

Table 2 The values of the extracted fit parameters $k = \mu^2/Q^2$, $f_2^{p-n}(1 \text{ GeV}^2)$ and μ_6 (in GeV^4), obtained by fitting the OPE expression (10), truncated at $D = 4$ ($\mu_6 \neq 0$). The notations are as in Table 1. See the text in Sect. 3.1 for explanation of the various $\chi^2/\text{d.o.f.}$'s

QCD variant	Q_{\min}^2 (fit)	k	$f_2^{p-n}(1.)$	μ_6	$\chi^2/\text{d.o.f.}$	$\chi_{\text{ext}}^2/\text{d.o.f.}$	$\chi_{0.268}^2/\text{d.o.f.}$	$\chi_{\text{all}}^2/\text{d.o.f.}$
$\overline{\text{MS}}$ pQCD	0.66	16	$-0.219 \pm 0.002 \pm 0.111$	$0.032 \pm 0.001 \pm 0.055$	7.31	53.4	2.92×10^5	1.68×10^6
(F)APT	0.66	0.063	$-0.198 \pm 0.002 \pm 0.106$	$0.018 \pm 0.001 \pm 0.028$	7.85	44.2	17.7	1.04×10^4
2 δ	0.66	0.999	$-0.116 \pm 0.002 \pm 0.094$	$0.014 \pm 0.001 \pm 0.023$	6.99	51.8	19.5	5.92×10^3
3 δ	0.66	4.46	$-0.101 \pm 0.002 \pm 0.114$	$0.013 \pm 0.001 \pm 0.025$	6.45	57.5	28.0	7.27×10^3
$\overline{\text{MS}}$ pQCD	0.47	16	$-0.216 \pm 0.002 \pm 0.120$	$0.031 \pm 0.001 \pm 0.045$	7.34	47.3	2.85×10^5	1.66×10^6
(F)APT	0.47	0.063	$-0.194 \pm 0.002 \pm 0.098$	$0.016 \pm 0.001 \pm 0.021$	7.65	35.6	10.0	6.95×10^3
2 δ	0.47	0.772	$-0.098 \pm 0.002 \pm 0.078$	$0.008 \pm 0.001 \pm 0.017$	6.88	48.2	7.42	1.40×10^3
3 δ	0.47	3.10	$-0.072 \pm 0.002 \pm 0.138$	$0.003 \pm 0.001 \pm 0.026$	6.64	53.5	6.56	218
$\overline{\text{MS}}$ pQCD	0.268	3.00	$-0.180 \pm 0.001 \pm 0.237$	$0.023 \pm 0.000 \pm 0.013$	6.52	38.7	6.52	∞
(F)APT	0.268	5.27	$-0.181 \pm 0.001 \pm 0.194$	$0.013 \pm 0.000 \pm 0.011$	7.77	37.0	7.77	3.91×10^3
2 δ	0.268	0.149	$-0.089 \pm 0.001 \pm 0.166$	$0.005 \pm 0.000 \pm 0.010$	6.27	41.9	6.27	293
3 δ	0.268	2.72	$-0.007 \pm 0.001 \pm 0.262$	$0.001 \pm 0.000 \pm 0.015$	5.99	46.5	5.99	47.3

reproduces approximately the QCD phenomenology at high energies (cf. also [17, 18]). A question appears whether the results of our fits in (F)APT depend significantly on this value. We repeated the analysis in (F)APT with the value $\bar{\Lambda}_{N_f=3} = 0.40 \text{ GeV}$, and it turned out that the results of the fits did not change significantly. For example, when $Q_{\min}^2 = 0.268 \text{ GeV}^2$ and $\mu_6 = 0$, we obtained $k = 2.86$ and the central value $f_2^{p-n}(1.) = -0.137$, and for the three quality parameters $\chi_{\text{ext}}^2/\text{d.o.f.}$, $\chi_{0.268}^2/\text{d.o.f.}$ and $\chi_{\text{all}}^2/\text{d.o.f.}$ the values 120., 54.7 and 878., respectively (to be compared with the corresponding values in Table 1, the third line from below). When $\mu_6 \neq 0$ in the fit, we obtained $k = 2.62$, $f_2^{p-n}(1.) = -0.187$, $\mu_6 = 0.013 \text{ GeV}^4$ and for the mentioned three quality parameters the values 42.3, 7.94 and 4.43×10^3 , respectively (to be compared with the corresponding values in Table 2, the third line from below).

When we add the parametrized elastic contribution of BSR, Eqs. (11)–(13), to the experimental points and to the theoretical curves of Fig. 3, we obtain the results presented in Fig. 4a, b. In comparison with Fig. 3, the values of BSR are shifted to significantly higher values at low Q^2 . With this approach, the quality of fits ($\chi^2/\text{d.o.f.}$) does not change, as we consider the elastic contribution as known (and parametrized) and added here simultaneously to the (inelastic) theoretical fitting curves and to the data points. This means that the results of Table 2 remain unchanged under this subsequent addition of $\Gamma_1^{p-n}(Q^2)_{\text{el.}}$.

We can observe in the results of Tables 1 and 2 that the values of the higher-twist parameters, $f_2^{p-n}(1)$ and μ_6 , are in the analytic variants of QCD smaller than in pQCD, this reduction being especially strong in the 3 δ QCD variant. It has been noted in the literature that in pQCD OPE there is a duality between the order of truncation of the leading-twist series and the higher-twist contribution [28–31, 50–57]: higher-twist contribution often significantly decreases with the inclusion of higher orders in the leading-twist part. This effect and ambiguity become stronger in the ranges where the perturbation theory becomes questionable (for example, at the large and low values of the Bjorken variable x , as it was shown in Refs. [62, 63], respectively). It has been observed that the higher-twist contribution is smaller, but also more stable (under the inclusion of more terms in the leading-twist), in QCD variants with infrared modifications of the coupling (various modifications lead to quite similar results [64, 65]). The latter probably incorporate a part of the higher-twist contributions (which are rather cumbersome [66]) into (formally) the leading-twist contribution for small x range at moderately small Q^2 values ($\lesssim 1 \text{ GeV}^2$) (see Ref. [67] and more recent studies [68–70] of the precise combined H1 and ZEUS data [71] for the DIS structure function F_2).

Following the above observations in Tables 1 and 2, we can conclude that the applications of the 2 δ and especially 3 δ

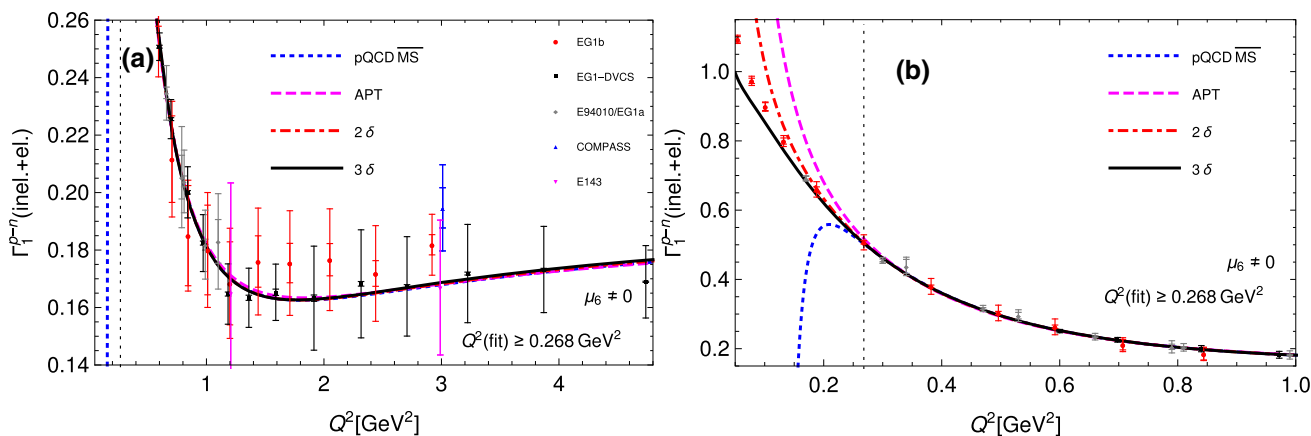


Fig. 4 As Fig. 3, but shifted upwards by the parametrized elastic contribution (11) [cf. also Eqs. (12)–(13)]

AQCD are very appropriate frameworks for the BSR studies because they appear to resum effectively a large part of the perturbative contribution into the leading-twist part (5). In this context, we wish to recall that 3δ AQCD is significantly different from the other two AQCD variants [(F)APT and 2δ AQCD] in the infrared region, because its coupling is not just finite there but goes to zero, $\mathcal{A}(Q^2) \sim Q^2 \rightarrow 0$, as motivated by large-volume lattice calculations, cf. [72–76] and Appendix C.2. Further, we wish to point out that the 2δ and 3δ AQCD couplings \mathcal{A} (and thus $\tilde{\mathcal{A}}_n$ and \mathcal{A}_n) are at large Q^2 indistinguishable from their underlying pQCD couplings a (\tilde{a}_n, a^n), cf. Eq. (C7), in contrast to (F)APT which satisfies the relation Eq. (B1) with $N = 1$. Therefore, theoretically, neither the higher-twist contribution of order $1/(Q^2)^N$ with $N \leq 4$ ($D \leq 8$), nor a part of it, is incorporated in the leading-twist contribution (5) in the 2δ and 3δ AQCD, in contrast to (F)APT. This indicates that the higher-twist terms extracted here with 2δ and 3δ AQCD (in truncated OPE) represent an effective form for the true higher-twist contribution with dimension $D \leq 8$ [and a part of the other ($D \geq 10$) presumably small contribution]. In pQCD this is definitely not so, because of the mentioned duality there between the order of truncation of the leading-twist series and the extracted higher-twist contribution. As a consequence, the extracted effective higher-twist contribution in pQCD represents a sum of the true higher-twist contribution and a significant part of the perturbative (leading-twist) contribution; this effective higher-twist contribution appears to be in general larger than the true higher-twist contribution.

3.3 Fits with “massive” OPE

For comparison, we performed a similar fit, but now with a “massive” higher-twist term instead of the truncated OPE expression (10)

$$\begin{aligned} \Gamma_1^{p-n, \text{mOPE}[4]}(Q^2; k, f_2^{p-n}(1); M^2) &= \left| \frac{g_A}{g_V} \right| \frac{1}{6} (1 - \mathcal{D}_{\text{BS}}(Q^2)) \\ &+ \frac{M_N^2}{(Q^2 + M^2)^2} \frac{1}{9} \left(a_2^{p-n} + 4d_2^{p-n} + 4f_2^{p-n}(Q^2) \right), \end{aligned} \tag{16}$$

where the squared mass M^2 in the denominator of the higher-twist part⁸ is taken to be constant (not running), and is expected to be $0 < M^2 \lesssim 1 \text{ GeV}^2$. Now, instead of $f_2^{p-n}(1)$ and μ_6 , the fit parameters are $f_2^{p-n}(1)$ and M^2 . The resulting curves, for $Q_{\text{min}}^2 = 0.268 \text{ GeV}^2$, are given in Fig. 5a, b, at the higher Q^2 and the lower $Q^2 < 1 \text{ GeV}^2$ momenta, respectively. The corresponding results are given in Table 3. These curves are analogous to those in the previous Fig. 3a, b in which the truncated OPE (10) was used. Numerically, the behavior at low Q^2 in the “massive” case is significantly influenced by the Q^2 -dependence of $f_2^{p-n}(Q^2)$. In the $\overline{\text{MS}}$ pQCD case, as in the $\overline{\text{MS}}$ pQCD cases of the analyses in all the Sections, we replaced in the higher-twist running parameter $f_2^{p-n}(Q^2)$ [cf. Eq. (8)] the scale Q^2 in an ad hoc way by the renormalization scale kQ^2 used in the leading-twist part ($k = 16$ resulted here), in order to artificially avoid the problem of Landau singularities in the pQCD coupling $a(Q^2)$. Comparing Fig. 5 and Table 3 with the corresponding “non-massive” case Fig. 3 and Table 2, we see that the results and extrapolations in the case of 3δ AQCD are now comparably good in the “massive” and the μ_4 & μ_6 approaches. Stated differently, the corresponding $\chi^2_{\text{fit}}/d.o.f.$ values in Tables 2 and 3 (with $Q_{\text{fit}}^2 = 0.268 \text{ GeV}^2$) are very similar. In the case of 2δ

⁸ Similar higher-twist expressions were used in the analyses of BSR in [77–79] where the leading-twist contribution was evaluated with the “Massive” Perturbation Theory (MPT) [80, 81]. MPT is an extension of APT [13–18] where, in contrast to APT, the coupling $\mathcal{A}(Q^2)$ is analytic in the point $Q^2 = 0$; nonetheless, the index N of Eq. (B1) (Appendix B) remains in MPT at the minimal value as in APT, i.e., $N = 1$.

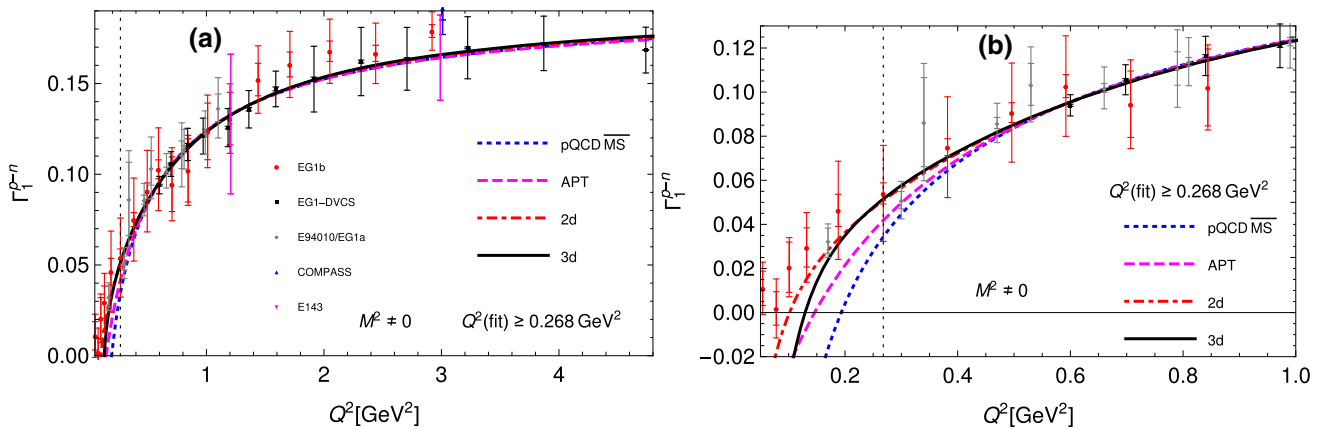


Fig. 5 As Fig. 3, but for the fit the OPE expression (16) with “massive” higher-twist term was used

Table 3 As in Table 2, but now the OPE form is “massive”, Eq. (16). The fits were made only for $Q_{\min}^2(\text{fit}) = 0.268 \text{ GeV}^2$. The extracted values of the squared mass M^2 are in GeV^2

QCD variant	$Q_{\min}^2(\text{fit})$	k	$f_2^{p-n}(1)$	M^2	$\chi^2/\text{d.o.f}$	$\chi_{\text{ext}}^2/\text{d.o.f}$	$\chi_{\text{all}}^2/\text{d.o.f}$
$\overline{\text{MS}}$ pQCD	0.268	16.0	$-0.286 \pm 0.003 \pm 1.035$	$0.623 \pm 0.017 \pm 0.471$	7.94	35.4	130
(F)APT	0.268	16.0	$-0.209 \pm 0.002 \pm 0.744$	$0.439 \pm 0.012 \pm 0.463$	7.48	31.5	31.2
2δ	0.268	0.689	$-0.097 \pm 0.002 \pm 0.155$	$0.336 \pm 0.023 \pm 0.371$	6.25	41.1	36.9
3δ	0.268	2.71	$-0.065 \pm 0.001 \pm 0.462$	$0.036 \pm 0.017 \pm 0.377$	5.99	46.6	55.0

\mathcal{A} QCD and (F)APT, the extrapolations are better in the “massive” than in the μ_4 & μ_6 approach, i.e., $\chi_{\text{all}}^2/\text{d.o.f.}$ is significantly reduced in the “massive” case. One reason for this lies perhaps in the fact that the massive higher-twist term is under control at very low Q^2 , unlike the separate $\mu_4(Q^2)/Q^2$ and $\mu_6/(Q^2)^2$ terms. Further, the extracted values of $f_2^{p-n}(1)$ are in general similar in the $\mu_6 = 0$, μ_4 & μ_6 and the “massive” approaches, although the uncertainties of the extracted parameters are quite high in the “massive” approach.⁹

The results of Table 3 show that the QCD variants with infrared-finite analytic coupling, and especially 3δ \mathcal{A} QCD, give smaller values of higher-twist parameters $f_2^{p-n}(1)$ and M^2 than pQCD. On the one hand, at low Q^2 , the smaller values of M^2 compensate partially the decreased value of f_2^{p-n} in the higher-twist contribution. On the other hand, smaller values of M^2 and $f_2^{p-n}(1)$ mean that at higher values of Q^2 the higher-twist contribution is significantly reduced; this can be seen also by expanding the massive higher-twist term of Eq. (16) in powers of M^2/Q^2 . Such effect is in full agreement with one observed in Refs. [28–31]; the effect can be considered as a stabilization of the higher-twist contribution. We also recall that 3δ \mathcal{A} QCD is significantly different from (F)APT and 2δ \mathcal{A} QCD in the infrared region, since its coupling goes to zero there, $\mathcal{A}(Q^2) \sim Q^2 \rightarrow 0$.

⁹ The systematic uncertainties of the extracted parameters in Table 3 are large and should therefore be regarded as crude estimates only, cf. comments in Appendix D.2.

It is possible to choose for the higher-twist term a massive form with a running mass, in the spirit of a dynamical effective gluon mass of the gluon propagator at low Q^2 [82]. Such masses appear in the literature often in definitions of QCD couplings at low Q^2 , and are responsible for the freezing (finiteness) of the coupling at $Q^2 \rightarrow 0$. The couplings in (F)APT and 2δ \mathcal{A} QCD have a freezing which could be described also via a running effective gluon mass. Our view is that the OPE higher-twist terms represent a new contribution not contained in the QCD coupling itself. The squared mass M^2 in such terms, Eq. (16), is considered constant, in the spirit of the approach of Ref. [77] (cf. also [78, 79]), where the basic component (delta function) in the spectral function of the higher-twist contribution gives such a mass term. Nonetheless, we repeated the aforementioned analysis for the case of a running squared mass $M^2(Q^2)$ representative of a dynamical effective gluon mass, chosen with a simple parametrization of Ref. [83]

$$M^2(Q^2) = \frac{m_0^2}{1 + (Q^2/\mathcal{M})^{1+p}} \quad (\mathcal{M} = 0.5 \text{ GeV}, p = 0.1), \tag{17}$$

where we chose for the parameters \mathcal{M} and p values within the expected regions [83]. The adjustable squared mass scale was taken (instead of m_0^2) to be $M^2(1 \text{ GeV}^2)$. The same analysis then gave the results presented in Table 4. We can see that the results are qualitatively similar to

Table 4 As in Table 3, but now the squared mass in the higher-twist term in Eq. (16) is running according to Eq. (17)

QCD variant	$Q^2_{\min}(\text{fit})$	k	$f_2^{p-n}(1.)$	$M^2(1 \text{ GeV}^2)$	$\chi^2/\text{d.o.f}$	$\chi^2_{\text{ext}}/\text{d.o.f}$	$\chi^2_{\text{all}}/\text{d.o.f}$
$\overline{\text{MS}}$ pQCD	0.268	11.9	$-0.214 \pm 0.002 \pm 0.651$	$0.240 \pm 0.010 \pm 0.272$	5.91	48.1	252
(F)APT	0.268	16.0	$-0.171 \pm 0.002 \pm 0.186$	$0.152 \pm 0.007 \pm 0.100$	6.65	43.2	38.8
2δ	0.268	9.26	$-0.160 \pm 0.002 \pm 0.496$	$0.277 \pm 0.011 \pm 0.318$	5.88	49.0	48.0
3δ	0.268	2.65	$-0.064 \pm 0.001 \pm 0.097$	$0.010 \pm 0.009 \pm 0.162$	5.99	46.5	48.3

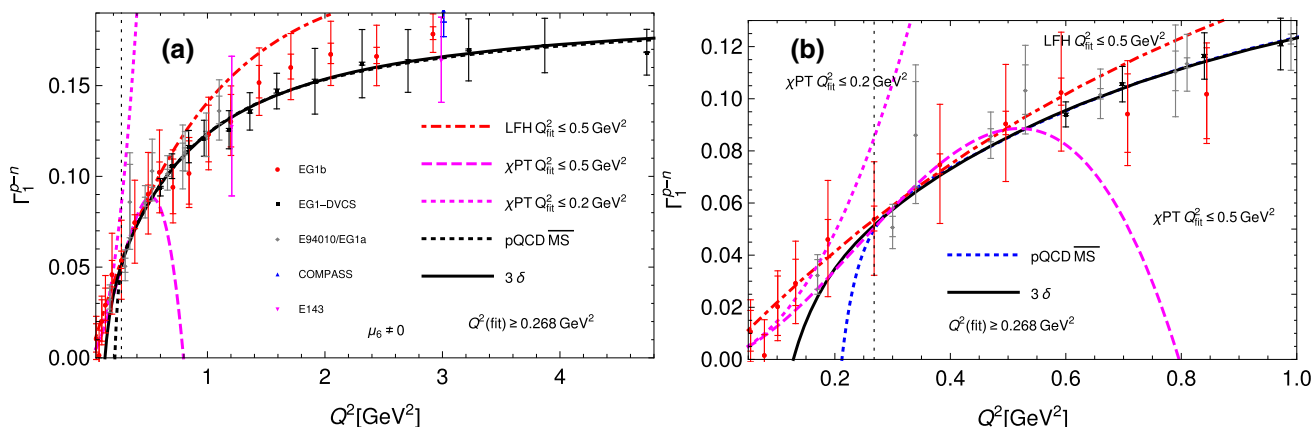


Fig. 6 As Fig. 3, but now with the low- Q^2 expressions (18) and (19) included. **b** is a zoomed-in version of **a**, for $Q^2 < 1 \text{ GeV}^2$. The lower bound of the fitting interval, $Q^2_{\min} = 0.268 \text{ GeV}^2$, is included as the thin dotted vertical line

those with the constant squared mass M^2 , Table 3, except that the values of $M^2(1 \text{ GeV}^2)$ are now lower. Nonetheless, a reasonable definition of the average squared mass value in the present analysis, for the considered fit interval $0.268 \text{ GeV}^2 < Q^2 < 3 \text{ GeV}^2$ may be $\langle M^2(Q^2) \rangle = (1/2) \times (M^2(0.268) + M^2(3)) \approx 1.52 \times M^2(1 \text{ GeV}^2)$. Or, if we regard that the squared mass is most relevant only in the low- Q^2 part $0.268 \text{ GeV}^2 < Q^2 < 1 \text{ GeV}^2$ of the fit interval, a reasonable definition of the average squared mass would be $\langle M^2(Q^2) \rangle = (1/2) \times (M^2(0.268) + M^2(1)) \approx 1.85 \times M^2(1 \text{ GeV}^2)$.

3.4 Testing low- Q^2 regime ansätze

At low Q^2 , the inelastic contribution to BSR behaves as $\sim Q^2$, according to Gerasimov–Drell–Hearn sum rule [84, 85] as pointed out and used in [28–31, 86–89]. Based on this, an expansion [4] motivated by chiral perturbation theory (χ PT) can be constructed

$$\Gamma_1^{p-n}(Q^2)_{\text{inel.}} = \frac{\chi_n^2 - \chi_p^2}{8M_N^2} Q^2 + A(Q^2)^2 + B(Q^2)^3 \quad (Q^2 \lesssim 0.5 \text{ GeV}^2), \quad (18)$$

where, according to Gerasimov–Drell–Hearn sum rule [84, 85], χ_n and χ_p are anomalous magnetic moments of nucleons [which appear also in the elastic BSR contributions, cf. Eq. (13)]; the parameters A and B are determined in the fit.

When we fit with this expression the inelastic BSR data [3–5] for $Q^2 \leq Q^2_{\max} = 0.2 \text{ GeV}^2$, we obtain $A = 0.765 \text{ GeV}^{-2}$ and $B = 0.678 \text{ GeV}^{-4}$, with $\chi^2(Q^2 \leq Q^2_{\max})/\text{d.o.f.} = 0.720$. On the other hand, if we take $Q^2_{\max} = 0.5 \text{ GeV}^2$ in the fitting, we obtain $A = 0.744 \text{ GeV}^{-2}$ and $B = -1.033 \text{ GeV}^{-4}$, $\chi^2(Q^2 \leq Q^2_{\max})/\text{d.o.f.} = 1.313$.

Another possible ansatz for the inelastic contribution to BSR at low Q^2 is the form of the light-front holographic (LFH) effective charge $\mathcal{A}^{(\text{LFH})}$ in the BSR (g_1) scheme [90, 91] [$\mathcal{A}(0)_{g_1} = 1$]

$$\begin{aligned} \Gamma_1^{p-n}(Q^2)_{\text{inel.}} &= \left| \frac{g_A}{g_V} \right| \frac{1}{6} \left[1 - \mathcal{A}^{(\text{LFH})}(Q^2) \right] \\ &= \left| \frac{g_A}{g_V} \right| \frac{1}{6} \left[1 - \exp\left(-\frac{Q^2}{2\kappa^2}\right) \right], \quad (Q^2 \lesssim 1 \text{ GeV}^2). \end{aligned} \quad (19)$$

When we fit with this expression the inelastic BSR data [3–5] for $Q^2 < Q^2_{\max} = 0.5 \text{ GeV}^2$, we obtain $\kappa = 0.479 \text{ GeV}$.¹⁰

In Fig. 6a, b, we present these low- Q^2 expressions. The $\overline{\text{MS}}$ pQCD and 3δ \mathcal{A} QCD curves (obtained from fit with $Q^2 \geq Q^2_{\min} = 0.268 \text{ GeV}^2$) are also included for comparison. In Fig. 6b we can see that the theoretical fitted curves of the presented QCD variants connect smoothly with the nonperturbative low- Q^2 curves (χ PT and LFH, both fitted

¹⁰ This is not far from the universal nonperturbative scale $\kappa = M_\rho/\sqrt{2} = 0.548 \text{ GeV}$, cf. [91].

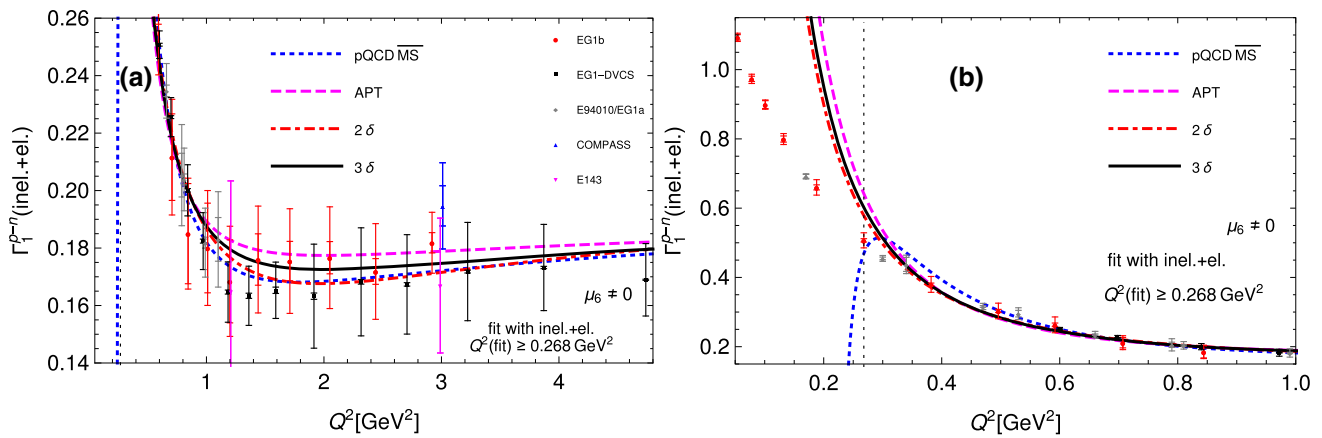


Fig. 7 As Fig. 3, but now the truncated (at $D = 4$) OPE expression (10) is fitted to the data for the total contribution $\Gamma_1^{p-n}(Q^2)_{\text{inel.+el.}}$. The lower bound of the fitting interval, $Q_{\text{min}}^2 = 0.268 \text{ GeV}^2$, is included as the thin dotted vertical line

to BSR up to $Q^2 = 0.5 \text{ GeV}^2$) at the values of Q^2 around 0.3 GeV^2 . Nonetheless, we recall that the apparent success of the ($\overline{\text{MS}}$) pQCD curve, down to about 0.3 GeV^2 , was achieved due to the ad hoc change of scale in $f_2^{p-n}(Q^2)$ to kQ^2 (with $k = 3$), to avoid the Landau singularities in the $D = 2$ term at $Q^2 \geq 0.268 \text{ GeV}^2$ (cf. also the discussion about that point in Sect. 3.2). We further notice that the 3δ QCD curve agrees well with the mentioned χ PT curve in a broader interval, $0.17 \text{ GeV}^2 < Q^2 < 0.3 \text{ GeV}^2$. Similar analyses with the goal of connecting the curves of pQCD (or of specific QCD variants) with nonperturbative curves at low Q^2 were performed in some of the references [28–31], in [92], and was discussed also in [93].

In Refs. [94,95], BSR at low $Q^2 < 0.3 \text{ GeV}^2$ was calculated with baryon chiral perturbation theory ($B\chi$ PT) up to NLO. The authors of [94,95] did not give the values of their parameters for BSR. However, careful visual comparison of their obtained Q^2 -dependence [cf. curves and bands in their Fig. 6(b) in Ref. [95]] with our χ PT curve (18) with $Q_{\text{fit}}^2 \leq 0.5 \text{ GeV}^2$ [the long-dashed curve in our Fig. 6b] shows very good agreement between them.

3.5 Fitting to total (inelastic + elastic) BSR data

We perform also the fitting of the truncated (at $D = 4$) OPE expression (10) to the data for the total BSR $\Gamma_1^{p-n}(Q^2)_{\text{inel.+el.}}$. As argued at the end of Sect. 2.3 [after Eq. (14)], such a fit has problematic aspects. These data are obtained by adding to the experimental data $\Gamma_1^{p-n}(Q_j^2)_{\text{inel.}}$ of Refs. [3–5] the parametrized elastic contribution Eqs. (11)–(13) of Ref. [60]. The uncertainties of the parametrized elastic form factors are considered to be less than 10% [60]. Since the elastic contribution (11) is quadratic in the form factors (and is numerically dominated by the proton contribution), the relative uncertainties of the elastic contribution

are less than 5%. Since we do not have more information about these uncertainties, we will neglect them in this analysis. This means that in the total BSR, we will consider that the statistical and the systematic uncertainties $\sigma_{j,\text{stat}}$ and $\sigma_{j,\text{sys}}$ are those of the inelastic contribution. Otherwise, the fitting is performed as in the previous Sect. 3.2.

The resulting curves are presented in Fig. 7a, b, for $Q^2 \geq Q_{\text{min}}^2$ with $Q_{\text{min}}^2 = 0.268 \text{ GeV}^2$. The obtained results are given in Table 5, for fits with various $Q_{\text{min}}^2 = 0.66, 0.47$ and 0.268 GeV^2 . Comparing the obtained results in Fig. 7 and Table 5 with the corresponding results in Fig. 4 and Table 2 (where the elastic part was not included in the fit procedure), we see that the inclusion of the elastic contribution in the fit procedure significantly deteriorates (increases) the values of the various fit quality parameters χ^2 , especially when the fit is performed in the larger interval ($Q_{\text{min}}^2 = 0.268 \text{ GeV}^2 \leq Q^2 < 3 \text{ GeV}^2$). In particular, the differences in quality are clearly visible when comparing Fig. 7b with Fig. 4b at low Q^2 . Only when Q_{min}^2 is relatively high, $Q_{\text{min}}^2 = 0.66 \text{ GeV}^2$, are some of the χ^2 parameters comparable in the two cases (but not the extrapolation quality parameters $\chi_{0.268}^2$ and χ_{all}^2). Further, the inclusion of the elastic contribution in the fit in general does not change significantly the extracted (mostly negative) values of $f_2^{p-n}(1 \text{ GeV}^2)$, but increases significantly the (positive) values of μ_6 .

For the fit analysis with the “massive” truncated OPE, Eq. (16), the results are presented in Table 6 for $Q_{\text{min}}^2 = 0.268 \text{ GeV}^2$. In general, the results are worse than in the corresponding “massive” OPE case fitted to the inelastic contribution (cf. Table 3 in Sect. 3.2). Namely, the extracted values of the parameter M^2 become negative ($M^2 \sim -0.1 \text{ GeV}^2$) and the fit quality values $\chi^2/\text{d.o.f.}$ are in general significantly higher than those in Table 3. The uncertainties of the extracted values of $f_2^{p-n}(1)$ and M^2 become reduced (in comparison to the case when the elastic part is not included

Table 5 As in Table 2, but now the fit is performed on the sum which includes the elastic contribution, i.e., on $\Gamma_1^{p-n}(\text{incl.} + \text{el.})$

QCD variant	Q_{\min}^2 (fit)	k	$f_2^{p-n}(1)$	μ_6	$\chi^2/\text{d.o.f.}$	$\chi_{\text{ext}}^2/\text{d.o.f.}$	$\chi_{0.268}^2/\text{d.o.f.}$	$\chi_{\text{all}}^2/\text{d.o.f.}$
$\overline{\text{MS}}$ pQCD	0.66	16	$-0.253 \pm 0.002 \pm 0.125$	$0.101 \pm 0.001 \pm 0.064$	7.11	55.6	3.65×10^5	1.26×10^6
(F)APT	0.66	16	$-0.227 \pm 0.002 \pm 0.105$	$0.086 \pm 0.001 \pm 0.028$	7.53	46.3	697	3.54×10^5
2 δ	0.66	0.487	$-0.121 \pm 0.002 \pm 0.057$	$0.073 \pm 0.001 \pm 0.011$	7.18	52.0	555	2.60×10^5
3 δ	0.66	2.01	$-0.095 \pm 0.002 \pm 0.145$	$0.067 \pm 0.001 \pm 0.033$	7.04	55.8	509	2.27×10^5
$\overline{\text{MS}}$ pQCD	0.47	1.37	$-0.194 \pm 0.002 \pm 0.111$	$0.114 \pm 0.001 \pm 0.056$	8.82	39.0	∞	∞
(F)APT	0.47	1.67	$-0.191 \pm 0.002 \pm 0.086$	$0.072 \pm 0.001 \pm 0.021$	19.4	63.4	364	2.46×10^5
2 δ	0.47	0.194	$-0.089 \pm 0.002 \pm 0.052$	$0.059 \pm 0.001 \pm 0.093$	14.8	57.8	250	1.67×10^5
3 δ	0.47	0.775	$-0.076 \pm 0.002 \pm 0.135$	$0.053 \pm 0.001 \pm 0.029$	12.6	44.9	193	1.38×10^5
$\overline{\text{MS}}$ pQCD	0.268	1.82	$-0.153 \pm 0.001 \pm 0.081$	$0.086 \pm 0.000 \pm 0.010$	28.0	82.3	28.0	∞
(F)APT	0.268	1.98	$-0.096 \pm 0.001 \pm 0.054$	$0.044 \pm 0.000 \pm 0.011$	131	254	131	8.84×10^4
2 δ	0.268	0.063	$0.018 \pm 0.001 \pm 0.042$	$0.028 \pm 0.000 \pm 0.006$	37.9	113	37.9	3.91×10^4
3 δ	0.268	0.846	$0.000 \pm 0.001 \pm 0.091$	$0.030 \pm 0.000 \pm 0.016$	68.7	145	68.7	4.61×10^4

in the fit); this is so because the elastic parts increase significantly BSR $\Gamma_1^{p-n}(Q^2)$ at low Q^2 where they are represented mostly by the “massive” higher-twist term, and hence the relative uncertainties of BSR at low Q^2 become smaller.

In addition to the massive case with constant squared mass M^2 , we include also the case of Q^2 -dependent squared mass Eq. (17) in the analysis with the elastic contribution included in the fit. The results for this case are presented in Table 7. These results are qualitatively similar to those with constant squared mass, Table 6; and the comparison of Table 7 with its counterpart Table 4 without the elastic contribution is similar to the above comparison when the squared mass is constant. We recall that an average mass in the Q^2 -independent case can be regarded to be $\langle M^2(Q^2) \rangle = (1/2) \times (M^2(0.268) + M^2(1)) \approx 1.85 \times M^2(1 \text{ GeV}^2)$.

4 Summary

Experimental results for the polarized Bjorken sum rule (BSR) $\Gamma_1^{p-n}(Q^2)$ were fitted, for various ranges of Q^2 , with OPE theoretical expressions using QCD couplings obtained in four different approaches: perturbative QCD (pQCD) in $\overline{\text{MS}}$ scheme; (Fractional) Analytic Perturbation Theory [(F)APT]; Two-delta \mathcal{A} QCD (2 δ); and Three-delta lattice-motivated \mathcal{A} QCD (3 δ). The QCD running coupling $\mathcal{A}(Q^2)$ in the latter three QCD variants does not have Landau singularities, in contrast to the pQCD coupling $a(Q^2) [\equiv \alpha_s(Q^2)/\pi]$.

In the fit of the inelastic experimental BSR results, up to two higher-twist terms [$\sim 1/Q^2, 1/(Q^2)^2$] were added to the theoretical leading-twist contribution. The elastic contributions, which are $\sim 1/(Q^2)^n$ with typically $n \geq 4$ at $Q^2 > 1 \text{ GeV}^2$, were then added by using the parametrization obtained from the literature. The fits were performed for the ranges $Q_{\min}^2 \leq Q^2 \leq 3 \text{ GeV}^2$, where $Q_{\min}^2 = 0.66, 0.47$ and 0.268 GeV^2 . In general, the best curves were obtained when 2 δ or 3 δ -couplings were used. When only $D = 2$ ($\sim 1/Q^2$) higher-twist term was included in the fit, the quality of the fitted curves, in the range of the fit and in the extrapolated ranges of Q^2 , in general did not depend significantly on Q_{\min}^2 of the fit. On the other hand, when both $D = 2$ and $D = 4$ terms were included, the quality in the extrapolated ranges of Q^2 was in general better for the lowest Q_{\min}^2 value (0.268 GeV^2), i.e., when the Q^2 -range of the fit was the largest. Comparably good results were obtained when “massive” higher-twist term was used in the OPE and the QCD coupling was either from (F)APT or 2 δ or 3 δ \mathcal{A} QCD.

When the range of fit had $Q_{\min}^2 = 0.268 \text{ GeV}^2$, the pQCD $\overline{\text{MS}}$ coupling approach worked and gave acceptable results only if the renormalization scale of the coupling was maintained everywhere at sufficiently high values, and the coefficient $f_2^{p-n}(Q^2) [\sim a(Q^2)^{\gamma_0/8\beta_0}]$ at the $D = 2$ term had an

Table 6 As in Table 3, i.e., the OPE form is “massive”, Eq. (16), but now the elastic part of BSR is included in the fit

QCD variant	Q_{\min}^2 (fit)	k	$f_2^{p-n}(1.)$	M^2	$\chi^2/\text{d.o.f}$	$\chi_{\text{ext}}^2/\text{d.o.f}$	$\chi_{\text{all}}^2/\text{d.o.f}$
$\overline{\text{MS}}$ pQCD	0.268	1.47	$0.117 \pm 0.000 \pm 0.042$	$-0.247 \pm 0.000 \pm 0.017$	384	795	∞
(F)APT	0.268	3.39	$0.041 \pm 0.001 \pm 0.032$	$-0.207 \pm 0.002 \pm 0.063$	395	760	4.63×10^3
2δ	0.268	0.063	$0.086 \pm 0.001 \pm 0.044$	$-0.156 \pm 0.002 \pm 0.032$	96.6	245	1.39×10^4
3δ	0.268	1.13	$0.083 \pm 0.001 \pm 0.082$	$-0.151 \pm 0.003 \pm 0.071$	143	320	1.05×10^4

Table 7 As in Table 6, but with Q^2 -dependent mass Eq. (17) in the higher-twist part of Eq. (16)

QCD variant	Q_{\min}^2 (fit)	k	$f_2^{p-n}(1.)$	$M^2(1 \text{ GeV}^2)$	$\chi^2/\text{d.o.f}$	$\chi_{\text{ext}}^2/\text{d.o.f}$	$\chi_{\text{all}}^2/\text{d.o.f}$
$\overline{\text{MS}}$ pQCD	0.268	4.88	$0.113 \pm 0.001 \pm 0.053$	$-0.065 \pm 0.001 \pm 0.070$	461	932	∞
(F)APT	0.268	3.22	$0.052 \pm 0.001 \pm 0.030$	$-0.072 \pm 0.001 \pm 0.034$	436	825	3.25×10^3
2δ	0.268	0.063	$0.102 \pm 0.001 \pm 0.034$	$-0.051 \pm 0.001 \pm 0.020$	119	288	6.58×10^5
3δ	0.268	1.14	$0.098 \pm 0.001 \pm 0.044$	$-0.048 \pm 0.001 \pm 0.023$	167	366	5.49×10^4

(ad hoc) increased scale $Q^2 \mapsto kQ^2$, in order to avoid the problem of the Landau singularities.

When the fit procedure was performed by fitting the theoretical OPE, truncated at $D = 4$ ($\sim 1/(Q^2)^2$) terms, to the sum of (experimental) inelastic and (parametrized) elastic BSR, the quality of the results turned out to be significantly worse in all the cases of the theoretical curves, something expected by the arguments presented at the end of Sect. 2.3. Namely, the elastic contribution is dominated by terms which behave at high values of Q^2 as $\sim 1/(Q^2)^{(D/2)}$ where usually $D \geq 8$, and these terms are not contained in the theoretical expressions for BSR which are usually OPE series truncated at $1/(Q^2)^2$.

The results of this work can be interpreted as an additional indication of the following important property: the evaluation of the (truncated) leading-twist contribution of spacelike low- Q^2 QCD observables such as inelastic BSR, in QCD variants 2δ and in particular 3δ AQCD [both have infrared finite and holomorphic coupling $\mathcal{A}(Q^2)$], appear to resum effectively a large part of the perturbative contribution of the observables, and leads to reduced extracted values of the higher-twist terms ($D = 2, 4$) in the truncated OPE. This property was noted earlier, for different observables, in Refs. [34, 35, 96]. In this context, it appears to be important that in 2δ and 3δ AQCD the coupling practically merges with the underlying pQCD coupling $a(Q^2)$ at higher values of $Q^2 \gg \Lambda_{\text{QCD}}^2$. This property is not shared by the (F)APT holomorphic coupling where the leading-twist series contains parts of the higher-twist contribution of as low dimensionality as $D = 2$. The extracted parameters in the higher-twist contribution, including those in the “massive” OPE, are especially reduced in 3δ AQCD. This suggests the possibility that the true higher-twist contribution is small, including the (sum of) terms of high dimension; and that the (truncated)

OPE with 3δ AQCD leading-twist gives, through fitting, an extracted value which is a good approximation to this true value of the higher-twist contribution. Numerically, the significantly reduced extracted value in (truncated) OPE with 3δ AQCD is probably partly related with the fact that 3δ AQCD differs from both 2δ and (F)APT AQCD variants in that its coupling goes to zero in the deep infrared regime, $\mathcal{A}^{(3\delta)}(Q^2) \sim Q^2 \rightarrow 0$. The latter property, we recall, is suggested by the large-volume lattice calculations of the dressing functions of the Landau-gauge gluon and ghost propagators at low Q^2 values.

Acknowledgements This work was supported by FONDECYT Postdoctoral Grant no. 3170116 (C.A.), by FONDECYT Regular Grant no. 1180344 (G.C. and C.A.), and by the RFBR Foundation through Grant no. 16-02-00790-a (A.V.K. and B.G.S.). We thank A. Deur, J. Blümlein and A. L. Kataev for helpful suggestions.

Open Access This article is distributed under the terms of the Creative Commons Attribution 4.0 International License (<http://creativecommons.org/licenses/by/4.0/>), which permits unrestricted use, distribution, and reproduction in any medium, provided you give appropriate credit to the original author(s) and the source, provide a link to the Creative Commons license, and indicate if changes were made. Funded by SCOAP³.

Appendix A: Renormalization scale and scheme dependence of the expansion coefficients

The dependence of the coupling $a(\mu^2) \equiv \alpha_s(\mu^2)/\pi$ (where $\mu^2 > 0$ means the spacelike region) is governed by the perturbative renormalization group equation (RGE)

$$\frac{\partial}{\partial \ln \mu^2} a(\mu^2) = -\beta_0 a(\mu^2)^2 - \beta_1 a(\mu^2)^3 - \beta_2 a(\mu^2)^4 - \dots, \tag{A1}$$

where in the mass-independent schemes the coefficients $\beta_0 = (11 - 2N_f/3)/4$ and $\beta_1 = (102 - 38N_f/3)/16$ are universal (scheme-independent), while the coefficients β_j (or equivalently, $c_j \equiv \beta_j/\beta_0$) for $j \geq 2$ are the (arbitrary) parameters which characterize the renormalization scheme.¹¹ The running of the coupling $a(\mu^2; c_2, c_3, \dots)$ with these scheme parameters is governed by the following relations (cf. App. A of Ref. [97], and App. A of Ref. [98]):

$$\begin{aligned} \frac{\partial a}{\partial c_2} &= a^3 + \mathcal{O}(a^5), & \frac{\partial a}{\partial c_3} &= \frac{1}{2}a^4 + \mathcal{O}(a^5), \\ \frac{\partial a}{\partial c_4} &= \mathcal{O}(a^5), \dots \end{aligned} \tag{A2}$$

When we use the relations (A1)–(A2) in the perturbation expansion (4) and account for the fact that $\mathcal{D}_{\text{BSR}}(Q^2)$ is a (spacelike) observable and thus independent of the scale μ^2 (i.e., independent of $k \equiv \mu^2/Q^2$) and of the scheme parameters c_j ($j \geq 2$), we obtain the following expressions for the perturbation coefficients d_j in terms of the general renormalization scale and scheme parameters (k, c_2, c_3):

$$d_1(k) = \bar{d}_1 + \beta_0 \ln k, \tag{A3a}$$

$$\begin{aligned} d_2(k; c_2) &= \bar{d}_2 + \bar{d}_1 2\beta_0 \ln k + \beta_0^2 \ln^2 k \\ &+ \beta_0 c_1 \ln k - (c_2 - \bar{c}_2); \end{aligned} \tag{A3b}$$

$$\begin{aligned} d_3(k; c_2, c_3) &= \left\{ \left[\bar{d}_3 + \bar{d}_2(3\beta_0 \ln k) + \bar{d}_1 \left(3\beta_0^2 \ln^2 k + 2\beta_0 c_1 \ln k \right) \right. \right. \\ &+ \left. \left(\beta_0^3 \ln^3 k + \frac{5}{2}\beta_0^2 c_1 \ln^2 k + \beta_0 \bar{c}_2 \ln k \right) \right] \\ &\left. - 2(c_2 - \bar{c}_2)(\bar{d}_1 + \beta_0 \ln k) - \frac{1}{2}(c_3 - \bar{c}_3) \right\}. \end{aligned} \tag{A3c}$$

Here we used the bar symbol to denote the choice of the scheme $\overline{\text{MS}}$ with the renormalization scale $\mu^2 = Q^2$ ($k = 1$). We recall that $k \equiv \mu^2/Q^2$ is the renormalization scale parameter ($0 < k \sim 1$), and that $\bar{c}_j \equiv \bar{\beta}_j/\beta_0$ ($j \geq 2$) are the $\overline{\text{MS}}$ scheme parameters.

Appendix B: Power analogs \mathcal{A}_n in AQCD

A QCD running coupling $\mathcal{A}(Q^2)$ which is holomorphic (analytic) in the non-timelike Q^2 complex plane sector ($-q^2 \equiv Q^2 \in \mathbb{C} \setminus (-\infty, -M_{\text{thr}}^2]$ (where $0 \leq M_{\text{thr}}^2 \lesssim 1 \text{ GeV}^2$), has in general nonperturbative (NP) contributions $\sim 1/(Q^2)^n$ appreciable at small $|Q^2|$. It differs from the underlying pQCD coupling $a(Q^2)$ by

$$\mathcal{A}(Q^2) - a(Q^2) \sim \left(\frac{\Lambda^2}{Q^2} \right)^N, \tag{B1}$$

¹¹ There is another scheme parameter, the scale Λ^2 , such that $a(\mu^2) = f(\mu^2/\Lambda^2)$. However, the change of Λ^2 can be regarded as the change in the definition of the renormalization scale μ^2 .

for $|Q^2| > \Lambda^2$ ($\gtrsim 0.1 \text{ GeV}^2$). Here, $N = 1$ in the case of (F)APT, and $N = 5$ in 2δ and 3δ AQCD. The analytization procedure can be presented schematically as $a(Q^2) \mapsto \mathcal{A}(Q^2)$. This procedure involves a and \mathcal{A} linearly (not as powers). Namely, when Q^2 is varied, $Q^2 \mapsto Q^2 + \Delta Q^2$, we have $a(Q^2 + \Delta Q^2) \mapsto \mathcal{A}(Q^2 + \Delta Q^2)$. Therefore,

$$\tilde{a}_n(Q^2) \mapsto \tilde{\mathcal{A}}_n(Q^2), \tag{B2}$$

where we denoted the (logarithmic) derivatives

$$\tilde{a}_n(Q^2) \equiv \frac{(-1)^{n-1}}{\beta_0^{n-1}(n-1)!} \left(Q^2 \frac{d}{dQ^2} \right)^{n-1} a(Q^2), \tag{B3a}$$

$$\begin{aligned} \tilde{\mathcal{A}}_n(Q^2) &\equiv \frac{(-1)^{n-1}}{\beta_0^{n-1}(n-1)!} \left(Q^2 \frac{d}{dQ^2} \right)^{n-1} \mathcal{A}(Q^2), \\ (n &= 1, 2, \dots). \end{aligned} \tag{B3b}$$

In this notation, $\tilde{a}_1 = a$ and $\tilde{\mathcal{A}}_1 \equiv \mathcal{A}$. We note that by pQCD RGE (A1) we have

$$\tilde{a}_n(Q^2) = a(Q^2)^n + \mathcal{O}(a^{n+1}). \tag{B4}$$

More specifically, we have

$$\tilde{a}_2 = a^2 + c_1 a^3 + c_2 a^4 + \dots, \tag{B5a}$$

$$\tilde{a}_3 = a^3 + \frac{5}{2}c_1 a^4 + \dots, \quad \tilde{a}_4 = a^4 + \dots, \quad \text{etc.}, \tag{B5b}$$

where, as mentioned in Appendix A, $c_j \equiv \beta_j/\beta_0$. When we invert these relations, we obtain

$$a^2 = \tilde{a}_2 - c_1 \tilde{a}_3 + \left(\frac{5}{2}c_1^2 - c_2 \right) \tilde{a}_4 + \dots, \tag{B6a}$$

$$a^3 = \tilde{a}_3 - \frac{5}{2}c_1 \tilde{a}_4 + \dots, \quad a^4 = \tilde{a}_4 + \dots, \quad \text{etc.} \tag{B6b}$$

The linearity of analytization, Eq. (B2), then gives us the analogs \mathcal{A}_n of the powers a^n

$$\mathcal{A}_2 = \tilde{\mathcal{A}}_2 - c_1 \tilde{\mathcal{A}}_3 + \left(\frac{5}{2}c_1^2 - c_2 \right) \tilde{\mathcal{A}}_4 + \dots, \tag{B7a}$$

$$\mathcal{A}_3 = \tilde{\mathcal{A}}_3 - \frac{5}{2}c_1 \tilde{\mathcal{A}}_4 + \dots, \quad \mathcal{A}_4 = \tilde{\mathcal{A}}_4 + \dots, \quad \text{etc.} \tag{B7b}$$

We note that in general $\mathcal{A}_n(Q^2) \neq \mathcal{A}(Q^2)^n$. The described construction (for $n = 1, 2, 3, \dots$) was performed in [45, 46].

The above approach was extended in Ref. [47] to the case of general real index $n = \nu$

$$\begin{aligned} \tilde{\mathcal{A}}_\nu(Q^2) &= \frac{1}{\pi} \frac{(-1)}{\beta_0^{\nu-1} \Gamma(\nu)} \int_0^\infty \frac{d\sigma}{\sigma} \rho_{\mathcal{A}}(\sigma) \text{Li}_{-\nu+1} \left(-\frac{\sigma}{Q^2} \right) \\ (0 < \nu), \end{aligned} \tag{B8}$$

where $\text{Li}_{-\nu+1}(z)$ is the polylogarithm function of order $-\nu + 1$, and $\rho_{\mathcal{A}}(\sigma) = \text{Im} \mathcal{A}(Q^2 = -\sigma - i\epsilon)$ is the cut discontinuity (spectral) function of \mathcal{A} . The coupling $\tilde{\mathcal{A}}_\nu$ can also be presented in an alternative form applicable in an extended

region $-1 < \nu$ (cf. [47] for details). The expression \mathcal{A}_ν , the analog of the power a^ν , was then obtained in the form

$$\mathcal{A}_\nu(Q^2) \equiv \tilde{\mathcal{A}}_\nu(Q^2) + \sum_{m=1,2,\dots} \tilde{k}_m(\nu) \tilde{\mathcal{A}}_{\nu+m}(Q^2) \quad (-1 < \nu), \tag{B9}$$

with the coefficients $\tilde{k}_m(\nu)$ given in Appendix A of Ref. [47]. Equation (B7) are a special case of Eq. (B9).

The perturbation expansion of the type Eq. (4) in Sect. 2.1, for any spacelike observable $\mathcal{D}(Q^2)$ in pQCD, can be reexpressed in terms of derivatives \tilde{a}_n of Eq. (B3a)

$$\mathcal{D}(Q^2)_{\text{mpt}} = a + \tilde{d}_1 \tilde{a}_2 + \tilde{d}_2 \tilde{a}_3 + \tilde{d}_3 \tilde{a}_4 + \mathcal{O}(\tilde{a}_5), \tag{B10}$$

where we denoted $a \equiv a(kQ^2; c_2, \dots)$, $\tilde{a}_n \equiv \tilde{a}_n(kQ^2; c_2, \dots)$, and the coefficients $\tilde{d}_n \equiv \tilde{d}_n(k; c_2, \dots, c_n)$ of this “modified” perturbation expansion (mpt) can be obtained by using the RGE-relations (B6)

$$\tilde{d}_1 = d_1, \quad \tilde{d}_2 = d_2 - c_1 d_1, \tag{B11a}$$

$$\tilde{d}_3 = d_3 - \frac{5}{2} c_1 d_2 + \left(\frac{5}{2} c_1^2 - c_2\right) d_1, \quad \text{etc.}, \tag{B11b}$$

and the coefficients $d_j \equiv d_j(k; c_2, \dots, c_j)$ are those of Eq. (A3). The expressions in $\mathcal{A}\text{QCD}$, corresponding to the perturbation expansions (B10) and (4), are then

$$\mathcal{D}(Q^2)_{\mathcal{A}\text{QCD}} = \mathcal{A} + \tilde{d}_1 \tilde{\mathcal{A}}_2 + \tilde{d}_2 \tilde{\mathcal{A}}_3 + \tilde{d}_3 \tilde{\mathcal{A}}_4 + \mathcal{O}(\tilde{\mathcal{A}}_5), \tag{B12a}$$

$$= \mathcal{A} + d_1 \mathcal{A}_2 + d_2 \mathcal{A}_3 + d_3 \mathcal{A}_4 + \mathcal{O}(\mathcal{A}_5). \tag{B12b}$$

The expansion (B12b) is written again, in a more detailed form, in Eq. (5) in Sect. 2.1. Both expressions (B12) are equivalent, but in practice it is more economical to do numerical evaluations using the expression (B12a).

We have $\mathcal{A}_n(Q^2) = \mathcal{A}(Q^2)^n$ only when $\mathcal{A}(Q^2)$ is a perturbative coupling, i.e., when it has no NP terms ($\sim 1/(Q^2)^m$). It is important not to use the power expansion in \mathcal{A} for the evaluation of spacelike observables. Namely, if we used power expansion in \mathcal{A} , the truncated series for $\mathcal{D}(Q^2)$ would have increasingly large (out of control) NP contributions when more power terms were included, and renormalization scale invariance would be increasingly violated, as emphasized in [99]. It turns out that in practice the sequence $\tilde{\mathcal{A}}_n(Q^2)$ ($n = 0, 1, 2, \dots$) is, in a general holomorphic $\mathcal{A}\text{QCD}$, a sequence with decreasing absolute values, at any finite Q^2 : $|\tilde{\mathcal{A}}_n(Q^2)| > |\tilde{\mathcal{A}}_{n+1}(Q^2)| > \dots$. In pQCD ($\tilde{a}_n(Q^2)$) this is in general not valid at low values $|Q^2| \lesssim 1 \text{ GeV}^2$.

Appendix C: QCD variants with holomorphic coupling $\mathcal{A}(Q^2)$

C.1 (Fractional) Analytic Perturbation Theory [(F)APT]

The pQCD running coupling $a(Q^2)$, in a given renormalization scheme (usually $\overline{\text{MS}}$), has in the complex Q^2 -plane cut along the real axis, $(-\infty, \Lambda_{\text{Lan}}^2)$, where $0 < \Lambda_{\text{Lan}}^2 \sim 0.1 \text{ GeV}^2$ is the branching point of the interval of the Landau singularities $(0, \Lambda_{\text{Lan}}^2)$ in the plane. Spacelike QCD observables $\mathcal{D}(Q^2)$ are holomorphic (analytic) functions of complex Q^2 , with the exception of the negative (timelike) semi-axis $(-\infty, -M_{\text{thr}}^2)$ where $0 \leq M_{\text{thr}}^2 \lesssim 1 \text{ GeV}^2$ is a threshold scale. The pQCD coupling $a(Q^2)$ does not reflect these properties, because of the mentioned cut interval $(0, \Lambda_{\text{Lan}}^2)$, called Landau singularities, on the positive semi-axis. Application of the Cauchy theorem to the integrand $a(Q'^2)/(Q'^2 - Q^2)$ in the complex Q'^2 -plane, with the use of the asymptotic freedom of QCD ($|a(Q'^2)| \rightarrow 0$ when $|Q'^2| \rightarrow \infty$), then gives the following dispersion integral for the value of the pQCD coupling $a(Q^2)$:

$$a(Q^2) = \frac{1}{\pi} \int_{-\Lambda_{\text{Lan}}^2 - \eta}^{+\infty} d\sigma \frac{\rho_1^{(\text{pt})}(\sigma)}{(\sigma + Q^2)}, \quad (\eta \rightarrow +0), \tag{C1}$$

where $\rho_1^{(\text{pt})}(\sigma) = \text{Im}a(Q'^2 = -\sigma - i\epsilon)$ is the cut discontinuity (spectral) function of $a(Q'^2)$. The elimination of the Landau cut contribution in this integral, while keeping the spectral function unchanged at other σ , then gives us the APT coupling [13, 14]

$$\mathcal{A}^{(\text{APT})}(Q^2) = \frac{1}{\pi} \int_0^{+\infty} d\sigma \frac{\rho_1^{(\text{pt})}(\sigma)}{(\sigma + Q^2)}, \tag{C2}$$

which has $M_{\text{thr}}^2 = 0$. It is straightforward to check that the difference $\mathcal{A}^{(\text{APT})}(Q^2) - a(Q^2)$ at large $|Q^2| > \Lambda_{\text{Lan}}^2$ remains appreciable, $\sim (\Lambda_{\text{Lan}}^2/Q^2)$, i.e., the index N in Eq. (B1) is $N = 1$.

The analog $\mathcal{A}_\nu^{(\text{APT})}(Q^2)$ of the power $a(Q^2)^\nu$ is then constructed in complete analogy, by replacing $\rho_1^{(\text{pt})}(\sigma)$ by $\rho_\nu^{(\text{pt})}(\sigma) = \text{Im}a(-\sigma - i\epsilon)^\nu$ [15, 17, 18]

$$\mathcal{A}_\nu^{(\text{APT})}(Q^2) = \frac{1}{\pi} \int_0^{+\infty} d\sigma \frac{\rho_\nu^{(\text{pt})}(\sigma)}{(\sigma + Q^2)}. \tag{C3}$$

We use in this work this form of (F)APT couplings \mathcal{A}_ν for $\nu = 1, 2, \dots$, in $\overline{\text{MS}}$ scheme. Specifically, we apply the underlying $\overline{\text{MS}}$ pQCD coupling $a(Q^2; \overline{\text{MS}})$ with $N_f = 3$ to evaluate $\rho_n^{(\text{pt})}$ and thus $\mathcal{A}_n^{(\text{APT})}(Q^2)$.

The authors of [19, 20] obtained explicit form of $\mathcal{A}_\nu^{(\text{APT})}(Q^2)$ at the one-loop level of the underlying pQCD coupling, and extended it to higher loop level by a perturbative approach [21–23]. This theory has the name Fractional Analytic Perturbation Theory (FAPT).

Numerical programs were constructed to calculate $A_v^{(APT)}(Q^2)$ up to four-loop level of the underlying \overline{MS} pQCD coupling a , in [100–102] in Maple and/or Fortran, and in [33, 103] in Mathematica.

We note that the general approach presented in Appendix B for calculation of A_v gives in the APT case (where $\rho_A(\sigma) = \rho_1^{(pt)}(\sigma)$, for $\sigma > 0$) approximately the same numerical results as the approach of Eq. (C3). If in the approach described in Appendix B we take into account in Eq. (B9) [or (B7) when $\nu = n$ is integer] a large number of terms $\tilde{A}_{\nu+m}$,¹² it turns out that the obtained $A_v(Q^2)$ numerically converges to that in Eq. (C3). We wish to stress that the approach presented in Appendix B works for any AQCD, i.e., QCD with any holomorphic $\mathcal{A}(Q^2)$, while the approach Eq. (C3) is applicable only in the (F)APT case, i.e., when $\rho_A(\sigma) = \rho_1^{(pt)}(\sigma)$.

The only adjustable parameter in (F)APT (with $N_f = 3$) is the scale $\bar{\Lambda}_{N_f=3}$ of the underlying QCD coupling $a(Q^2) = f(Q^2/\bar{\Lambda}_3^2)$; the high energy QCD is approximately reproduced with $N_f = 3$ (F)APT when $\bar{\Lambda}_3 = 0.45$ GeV (cf. also Ref. [17, 18]); we use this value in our analysis, but we also comment on the case $\bar{\Lambda}_3 = 0.40$ GeV.

C.2 2δ and 3δ AQCD

This type of QCD variants [32, 34, 35] with coupling $\mathcal{A}(Q^2)$ holomorphic in $Q^2 \in \mathbb{C} \setminus (-\infty, -M_{thr}^2]$ are constructed on the idea that: (a) the coupling $\mathcal{A}(Q^2)$ at high $|Q^2| > 1$ GeV² should practically coincide with the underlying pQCD¹³ coupling $a(Q^2)$; (b) and at moderate and low $|Q^2| \lesssim 1$ GeV² the coupling should reproduce the well measured semihadronic τ -lepton decay physics and possibly some other experimental indicators. We note that (F)APT does not fulfill these requirements.

The condition (a) then implies that the spectral function $\rho_A(\sigma) \equiv \text{Im}\mathcal{A}(-\sigma - i\epsilon)$ is at large $\sigma > 1$ GeV² (approximately) equal to the spectral function of the underlying pQCD, $\rho_a(\sigma) \equiv \rho_1^{(pt)}(\sigma) \equiv \text{Im}a(-\sigma - i\epsilon)$. At low positive σ , the unknown behavior of the spectral function $\rho_A(\sigma)$ is parametrized as a sum of delta functions

$$\rho_A^{(n\delta)}(\sigma) = \pi \sum_{j=1}^n \mathcal{F}_j \delta(\sigma - M_j^2) + \Theta(\sigma - M_0^2) \rho_1^{(pt)}(\sigma). \tag{C4}$$

¹² This is in principle not necessary; if, for example, a physical quantity $\mathcal{D}(Q^2)$ is calculated up to $\mathcal{O}(a^4) \mapsto \mathcal{O}(A_4)$, then only terms up to \mathcal{A}_4 are in principle needed on the right-hand sides of Eq. (B7).

¹³ This means that in Eq. (B1) the index N is large; as a consequence, the well demonstrated success of pQCD at high momenta is reproduced in AQCD.

Implicitly, we expect $M_1^2 < M_2^2 < \dots < M_n^2 < M_0^2$, where $M_1^2 = M_{thr}^2$ is the mentioned threshold scale (expected to be $\sim m_\pi^2 \sim 10^{-2}$ GeV²), and M_0^2 (~ 1 GeV²) can be called the pQCD-onset scale. Application of the Cauchy theorem then gives for the coupling the expression

$$A^{(n\delta)}(Q^2) \left(\equiv \frac{1}{\pi} \int_0^\infty d\sigma \frac{\rho_A(\sigma)}{(\sigma + Q^2)} \right) = \sum_{j=1}^n \frac{\mathcal{F}_j}{(Q^2 + M_j^2)} + \frac{1}{\pi} \int_{M_0^2}^\infty d\sigma \frac{\rho_1^{(pt)}(\sigma)}{(Q^2 + \sigma)}. \tag{C5}$$

The parametrization with n delta functions in Eq. (C4) means that the part $\Delta\mathcal{A}$ of the QCD coupling originating from the unknown low- σ part of the spectrum is parametrized by a near-diagonal Padé $[n - 1/n](Q^2)$ approximant

$$\Delta\mathcal{A}(Q^2) \equiv \frac{1}{\pi} \int_0^{M_0^2} d\sigma \frac{\rho_A(\sigma)}{(Q^2 + \sigma)} \mapsto \sum_{j=1}^n \frac{\mathcal{F}_j}{(Q^2 + M_j^2)} = \frac{P_{n-1}(Q^2)}{Q_n(Q^2)} \equiv [n - 1/n]_{\Delta\mathcal{A}}(Q^2), \tag{C6}$$

where P_{n-1} and Q_n are polynomials of degree $n - 1$ and n in Q^2 , respectively. If $\Delta\mathcal{A}$ is a Stieltjes function,¹⁴ a theorem in the Padé theory [104] (cf. also [105]) states that there exists a sequence of Padé approximants $[n - 1/n](Q^2)$ which converges to $\Delta\mathcal{A}(Q^2)$ for any $Q^2 \in \mathbb{C} \setminus (-\infty, -M_{thr}^2]$ when n increases (if $\Delta\mathcal{A}$ is not Stieltjes, it is not known whether such a convergence is guaranteed).

The underlying pQCD coupling $a(Q^2)$ is determined, to a rather high degree of accuracy, by the world average value $a(Q^2 = M_Z^2; \overline{MS}) = 0.1185/\pi$ [61]. We use this value, and we RGE-evolve $a(\overline{MS})$ to lower values of $|Q^2|$, by using the four-loop RGE (A1) and three-loop quark mass threshold conditions [106] in \overline{MS} , into the region of interest where $N_f = 3$; subsequently, we change the coupling $a(Q^2; \overline{MS})$ to the considered renormalization scheme to obtain the underlying coupling $a(Q^2)$; cf. [35] for more details. Thus we also obtain the perturbative spectral function $\rho_1^{(pt)}(\sigma) = \text{Im}a(Q^2 = -\sigma - i\epsilon)$, in the considered scheme and for $N_f = 3$.

At that point, the considered AQCD, Eqs. (C4)–(C5) has altogether $(2n + 1)$ parameters, namely \mathcal{F}_j and M_j^2 ($j = 1, \dots, n$) and the pQCD-onset scale M_0^2 . These are to be fixed by the conditions (a) and (b) for $\mathcal{A}(Q^2)$ at high and low $|Q^2|$ mentioned at the beginning of this Section C.2. The condition (a) is implemented by requiring a large index value for the difference Eq. (B1); in our considered cases of 2δ and 3δ coupling we took $N = 5$

$$\mathcal{A}(Q^2) - a(Q^2) \sim \left(\frac{\Lambda^2}{Q^2} \right)^5. \tag{C7}$$

¹⁴ If $\rho_A(\sigma) \geq 0$ for $\sigma > 0$, then $\mathcal{A}(Q^2)$ and $\Delta\mathcal{A}(Q^2)$ are Stieltjes functions.

Table 8 Values of the parameters of 2δ and 3δ coupling used in the present work, for $N_f = 3$: the Lambert Λ_L scale (in GeV); and the dimensionless parameters $s_j \equiv M_j^2/\Lambda_L^2$ and $f_j \equiv \mathcal{F}_j/\Lambda_L^2$. The

“input” parameter choice is $\alpha_s(M_Z^2; \overline{\text{MS}}) = 0.1185$ and $r_\tau^{(D=0)} = 0.201$. 2δ coupling is in the Lambert scheme with $c_2 = -4.9$; 3δ coupling is in the four-loop LMM scheme. We refer for details to [33,35]

AQCD	$\bar{\alpha}_s(M_Z^2)$	$r_\tau^{(D=0)}$	s_1	s_2	s_3	f_1	f_2	f_3	s_0	Λ_L [GeV]	$\pi \mathcal{A}_{\text{max}}$
2δ	0.1185	0.201	18.734	1.0361	–	0.2929	0.5747	–	25.610	0.2564	2.0713
3δ	0.1185	0.201	3.970	18.495	474.20	–2.8603	11.801	5.2543	652	0.11564	0.9156

This represents altogether four conditions (for each increase of N by one, from $N = 1$, there is one condition).

When we take $n = 2$, i.e., two delta functions in the spectral function (C4), we have five parameters to determine; therefore one additional condition is needed. This condition will be the reproduction of the measured values of the quantity $r_\tau^{(D=0)}$, the semihadronic strangeless τ decay rate ratio (the leading-twist part, and with mass effects subtracted).¹⁵ Its experimental value is approximately in the range 0.201 ± 0.002 . Its theoretical expression can be represented as a weighted contour integral of the (massless) Adler function¹⁶ $d(Q^2)$

$$r_{\tau,\text{th}}^{(D=0)} = \frac{1}{2\pi} \int_{-\pi}^{+\pi} d\phi (1 + e^{i\phi})^3 (1 - e^{i\phi}) \times d(Q^2 = m_\tau^2 e^{i\phi}; D = 0) \quad (\approx 0.201 \pm 0.001). \quad (\text{C8})$$

We refer to [32,34,35] for details. In the $n = 2$ case (2δ AQCD), we still have the freedom of choosing the renormalization scheme. We took it as the Lambert scheme ($c_j = c_2^{j-1}/c_1^{j-2}$, for $j \geq 3$), with $c_2 = -4.9$ [33]. It is possible to vary the value of c_2 , but when it is different by several units from this value, either the pQCD-onset scale M_0 becomes appreciably higher than ≈ 1 GeV, or the value $\mathcal{A}(0)$ becomes larger than one, cf. Table 2 of [33].

When we take $n = 3$, i.e., three delta functions in the spectral function (C4), there are two additional parameters to be fixed. These two parameters are fixed by the condition $\mathcal{A}(Q^2) \sim Q^2$ when $Q^2 \rightarrow 0$ and the local maximum of $\mathcal{A}(Q^2)$ achieved at $Q^2 \approx 0.135$ GeV². These conditions are motivated by the results of lattice calculations of the gluon and ghost dressing functions in the Landau gauge at low positive Q^2 [72] (cf. also [73]).¹⁷ In our couplings we use throughout $N_f = 3$, which makes them applica-

ble in the regions $|Q^2| < 3$ GeV². The lattice calculations were performed in the MiniMOM renormalization scheme (MM) [110–114]. Our coupling $\mathcal{A}(Q^2)$ was constructed in the $N_f = 3$ MM scheme, but rescaled from the MM scale convention (Λ_{MM}) to the usual scale convention ($\Lambda_{\overline{\text{MS}}}$), the latter representing what we call Lambert MM (LMM) scheme. In [34] we used the three-loop LMM, and in [35] the four-loop LMM scheme. In the present work we use the latter (four-loop LMM) scheme, i.e., the coupling from [35].

In Table 8 we specify the parameters of the 2δ AQCD [32,33] and 3δ AQCD coupling [35], used in the present work. The values of the parameters of the 2δ coupling, with $c_2 = -4.9$, are slightly different from the corresponding values in [33] (Table 2 there, third line), because there we used $\alpha_s(M_Z^2; \overline{\text{MS}}) = 0.1184$ and $r_\tau^{(D=0)} = 0.203$, while here we use $\alpha_s(M_Z^2; \overline{\text{MS}}) = 0.1185$ and $r_\tau^{(D=0)} = 0.201$. We note that the maximal value of $\mathcal{A}(Q^2)$ for positive Q^2 is achieved in the 2δ case at $Q^2 = 0$: $\pi \mathcal{A}^{(2\delta)}(0) = 2.0713$; and in the 3δ case at $Q^2 = Q_0^2 = 0.1348$ GeV²: $\pi \mathcal{A}^{(3\delta)}(Q_0^2) = 0.9156$. The pQCD-onset scales are $M_0 = \sqrt{s_0} \Lambda_L = 1.298$ GeV and 2.953 GeV, respectively.

Other QCD running couplings $\mathcal{A}(Q^2)$ without Landau singularities have been constructed in the literature, some of them having at $Q^2 = 0$ zero value $\mathcal{A}(0) = 0$ [115–119], finite nonzero value (for reviews, cf. [38,120]), or infinite value [121–124]. The construction of such couplings is mostly based on the dispersive approaches similar to the ones described in this Appendix; however, such kind of dispersive approaches can also be applied to entire physical observables, cf. [16,118,119,125–135]. Yet another approach is the Light Front Holographic (LFH) QCD [90,91], where the coupling $\mathcal{A}^{(\text{LFH})}(Q^2)$ has the form $\exp(-Q^2/2\kappa^2)$ at low positive Q^2 , cf. Eq. (19), and can be extended to higher positive Q^2 by matching of $\mathcal{A}(Q^2)$ and $d\mathcal{A}(Q^2)/dQ^2$ at a matching scale $Q_0 \sim 1$ GeV² to pQCD [92].

¹⁵ Higher-twist contributions in r_τ decay ratio are known to be strongly suppressed.

¹⁶ This is the canonical Adler function with $N_f = 3$, i.e., it is normalized in such a way that $d(Q^2)_{\text{pt}} = a(Q^2) + \mathcal{O}(a^2)$.

¹⁷ The calculation in [72,73] were performed for $N_f = 0$ case. They are similar to the results when $N_f = 2, 4$ [74–76] although these results are not so precise. If the running is defined via the mentioned dressing functions, the mentioned conditions, with $\mathcal{A}(0) = 0$, follow. Different definitions involving, in addition, a dynamical gluon mass [107–109], would imply $\mathcal{A}(0) > 0$, which holds also in 2δ AQCD and in (F)APT,

Footnote 17 continued with the values $\mathcal{A}(0) = 2.0713, 1.3963$, respectively (for $N_f = 3$). For a discussion on these issues, we refer to [35].

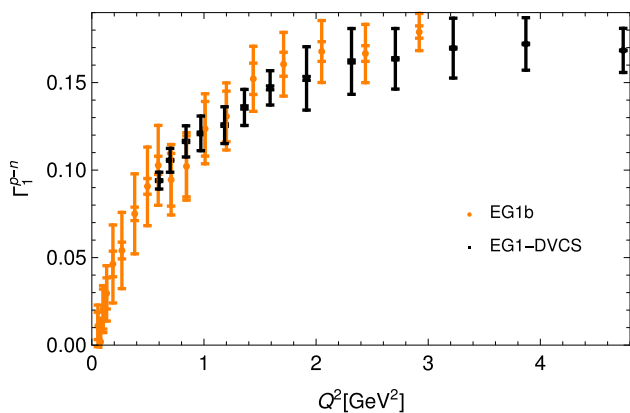


Fig. 8 Experimental points $\Gamma_1^{p-n}(Q_j^2; \text{inel})$ for two of the considered experiments: EG1b [4] (lighter) and EG1-DVCS [5] (darker). The smaller uncertainties are statistical, $\delta\Gamma_1^{p-n}(Q_j^2; \text{inel})_{\text{stat}} = \sigma_{j,\text{stat}}$; the larger are systematic, $\delta\Gamma_1^{p-n}(Q_j^2; \text{inel})_{\text{sys}} = \sigma_{j,\text{sys}}$. We note that the EG1-DVCS points have very small statistical uncertainties $\sigma_{j,\text{stat}}$ (the resolution of the figure is too small to see them)

Appendix D: Uncertainties of extracted values of f_2^{p-n} and μ_6 : statistical and systematic

The experimental data in the fit procedure are $\Gamma_1^{p-n}(Q_j^2; \text{inel})_{\text{exp.}}$. The leading-twist part of the (theoretical) OPE expression (10) has no fit parameters in our approach, apart from the renormalization scale parameter $k \equiv \mu^2/Q^2$. The latter parameter will be kept fixed at its value obtained by the approach of minimization of χ^2 . We will use the following notation:

$$z_j \equiv 1/Q_j^2, \quad y_j \equiv \Gamma_1^{p-n}(Q_j^2; \text{inel})_{\text{exp.}} - \Gamma_1^{p-n}(Q_j^2)_{\text{theor.}}^{(\text{LT})} \tag{D1}$$

In order to estimate the uncertainties of the extracted parameters $f_2^{p-n}(1)$ and μ_6 , we will consider for simplicity that not just μ_6 but also f_2^{p-n} does not run (i.e., that μ_4 does not run) with Q^2 . Further, we will make the following approximations: the statistical uncertainties at different points will be considered as completely uncorrelated; the systematic uncertainties at different points will be considered as completely correlated within one experiment, and completely uncorrelated between two different experiments. The systematic uncertainties $\delta\Gamma_1^{p-n}(Q_j^2; \text{inel})_{\text{sys}}$ are in general significantly larger than the statistical uncertainties $\delta\Gamma_1^{p-n}(Q_j^2; \text{inel})_{\text{stat}}$, cf. Fig. 8.

D.1 $\mu_6 = 0$ case

First we will consider the case when $\mu_6 = 0$ (and f_2^{p-n} is not running with Q^2). We will estimate the uncertainty of f_2^{p-n} due to the statistical uncertainties $\sigma_{j,\text{stat}}$ at Q_j^2 's and then due to the systematic uncertainties $\sigma_{j,\text{sys}}$. The renormal-

ization scheme parameter k will be kept fixed during these estimations.

In this approach, the considered χ^2 is

$$\chi^2(\mu_4) = \sum_j w_j (y_j - \mu_4 z_j)^2, \tag{D2}$$

where we will denote

$$w_j \equiv \frac{1}{\sigma_{j,\text{stat}}^2}, \tag{D3}$$

i.e., the squared statistical uncertainty at the measured point Q_j^2 . The minimization of χ^2 then gives the extracted value of μ_4

$$\frac{\partial \chi^2(\mu_4)}{\partial \mu_4} \Big|_{\mu_4 = \hat{\mu}_4} = 0 \Rightarrow \hat{\mu}_4 = \frac{\overline{y z}}{z^2}, \tag{D4}$$

where we will use throughout the notation for the unnormalized ‘‘average’’

$$\overline{A} \equiv \sum_j w_j A(z_j) = \sum_j \frac{1}{\sigma_{j,\text{stat}}^2} A(z_j). \tag{D5}$$

Since the deviations of $y_j \equiv y(z_j)$ due to statistical uncertainties are considered independent at different z_j , the rule of the sum of the squares of standard deviations is valid. It is then straightforward to deduce the square of the standard deviation for $\hat{\mu}_4$.

$$\sigma^2(\hat{\mu}_4)_{\text{stat}} = \frac{1}{z^2}. \tag{D6}$$

Then it can be checked, by Taylor expansion of $\chi^2(\mu_4)$ around the point $\hat{\mu}_4$ up to the terms $(\delta\mu_4)^2$, that the following (approximate) relation holds:

$$\chi^2(\mu_4 = \hat{\mu}_4 \pm \sigma(\hat{\mu}_4)_{\text{stat}}) = \chi^2(\hat{\mu}_4) + 1. \tag{D7}$$

Any of the two relations (D6)–(D7) can be used to evaluate the uncertainty $(\delta\hat{\mu}_4)_{\text{stat}} \equiv \sigma(\hat{\mu}_4)_{\text{stat}}$. We used the relation (D7), which gives us in practice somewhat higher values of the uncertainty.¹⁸ Further, using the relation (6) at $Q^2 = 1 \text{ GeV}^2$, this then gives us the uncertainty $(\delta\hat{f}_2)_{\text{stat}}$ ¹⁹

$$(\delta\hat{f}_2)_{\text{stat}} \equiv \sigma(\hat{f}_2)_{\text{stat}} = \frac{9}{4M_N^2} \sigma(\hat{\mu}_4)_{\text{stat}} = \frac{9}{4M_N^2} \frac{1}{z^2}. \tag{D8}$$

The systematic uncertainties were estimated in the following way. For simplicity we consider for this only two experiments, namely EG1b [4] (experiment ‘‘1’’) and the newer

¹⁸ This difference, of a few percent ($\leq 5\%$), is presumably principally due to the effect of the running of $\mu_4(Q^2)$ with Q^2 , the effect not accounted for in the formula (D6).

¹⁹ We denote, from here on, by \hat{f}_2 the value of $f_2^{p-n}(1 \text{ GeV}^2)$ extracted by the fit procedure.

JLAB EG1-DVCS results [5] (experiment “2”), in the interval $0 < Q^2 < 3 \text{ GeV}^2$. These two experiments represent most of the available data points, and each of them covers most of the mentioned Q^2 -interval. In each experiment, the systematic uncertainties at different points will be considered as strongly correlated, in the sense that in each experiment we will estimate the systematic uncertainty of \hat{f}_2 as the one obtained by averaging the deviations

$$(\delta \hat{f}_2)_{\text{sys}}^{(E)} \equiv \sigma(\hat{f}_2)_{\text{sys}}^{(E)} \approx \frac{1}{2} \left(|\hat{f}_2(\text{UP})^{(E)} - \hat{f}_2^{(E)}| + |\hat{f}_2(\text{DO})^{(E)} - \hat{f}_2^{(E)}| \right), \tag{D9}$$

where E is the experiment ($E = 1$ or $E = 2$); “UP” refers to the value of $f_2^{p-n}(1\text{GeV}^2)$ extracted from the data of the experiment increased by $\sigma_{j,\text{sys}}$ at the points Q_j^2 of the experiment, i.e., $\Gamma_1^{p-n}(Q_j^2; \text{incl.}) + \sigma_{j,\text{sys}}$; analogously, “DO” refers to the value extracted from $\Gamma_1^{p-n}(Q_j^2; \text{incl.}) - \sigma_{j,\text{sys}}$; and $\hat{f}_2^{(E)}$ is the value of $f_2^{p-n}(1\text{GeV}^2)$ extracted from the central points $\Gamma_1^{p-n}(Q_j^2; \text{incl.})$ of the experiment.

Having these estimates, the question is with what relative weights to combine the two systematic uncertainties $(\delta \hat{f}_2)_{\text{sys}}^{(E)}$ for $E = 1$ and $E = 2$. This will be obtained by combining the unnormalized averages of the expressions appearing in $\hat{\mu}_4^{(E)}$ of the two experiments, and assuming that the (systematic) deviations for $\hat{\mu}_4^{(E)}$ of the two experiments are mutually independent. Namely, using the definition of the (unnormalized) averages, Eq. (D5), for the two experiments, we have the identities

$$\bar{A} \equiv \sum_j w_j A(z_j) = \bar{A}^{(1)} + \bar{A}^{(2)}. \tag{D10}$$

Applying these identities to $\bar{y}z$ and \bar{z}^2 in Eq. (D4), we obtain

$$\hat{\mu}_4 = \frac{\bar{y}z}{\bar{z}^2} = \frac{\bar{y}z^{(1)} + \bar{y}z^{(2)}}{\bar{z}^{2(1)} + \bar{z}^{2(2)}} = \alpha \hat{\mu}_4^{(1)} + (1 - \alpha) \hat{\mu}_4^{(2)}, \tag{D11}$$

where

$$\alpha = \frac{1}{\left(1 + \frac{\bar{z}^{2(2)}}{\bar{z}^{2(1)}} \right)}. \tag{D12}$$

The assumption (approximation) that the two systematic deviations of $\hat{\mu}_4$ of experiments 1 and 2 are independent, then leads us to the standard deviation $(\delta \hat{\mu}_4)_{\text{sys}}$

$$(\delta \hat{\mu}_4)_{\text{sys}} \equiv \sigma(\hat{\mu}_4)_{\text{sys}} = \left[\alpha^2 \sigma^2(\hat{\mu}_4)_{\text{sys}}^{(1)} + (1 - \alpha)^2 \sigma^2(\hat{\mu}_4)_{\text{sys}}^{(2)} \right]^{1/2}, \tag{D13}$$

and by relation (6) analogously

$$(\delta \hat{f}_2)_{\text{sys}} \equiv \sigma(\hat{f}_2)_{\text{sys}} = \left[\alpha^2 \sigma^2(\hat{f}_2)_{\text{sys}}^{(1)} + (1 - \alpha)^2 \sigma^2(\hat{f}_2)_{\text{sys}}^{(2)} \right]^{1/2}, \tag{D14}$$

where the estimates $\sigma(\hat{f}_2)_{\text{sys}}^{(E)}$ ($E = 1, 2$) are given in Eq. (D9). Eq. (D14) represents thus an estimate of the uncertainty of the extracted value of $f_2^{p-n}(1\text{GeV}^2)$ due to systematic uncertainties of the experimental data. In practice, it turns out that this uncertainty is dominated by the results of the experiment 2 (JLAB EG1-DVCS) [5], i.e., $(1 - \alpha) \approx 1$. This is so because $\bar{z}^{2(2)} \gg \bar{z}^{2(1)}$, since the experiment 2 has significantly larger values of w_j , i.e., significantly smaller values of $\sigma_{j,\text{stat}}^2$.

D.2 $\mu_6 \neq 0$ case

When the coefficient μ_6 is included in the truncated OPE (10) as a fit parameter, the analysis is analogous to the previous Sec. D.1, except that now the algebra is more involved. The values of $\hat{\mu}_4$ and $\hat{\mu}_6$ are obtained by simultaneous minimization of

$$\chi^2(\mu_4, \mu_6) = \sum_j w_j (y_j - \mu_4 z_j - \mu_6 z_j^2)^2, \tag{D15}$$

with respect to μ_4 and μ_6 . This gives

$$\hat{\mu}_4 = \frac{-y\bar{z}^2 \bar{z}^3 + \bar{y}z \bar{z}^4}{D}, \quad \hat{\mu}_6 = \frac{y\bar{z}^2 \bar{z}^2 - \bar{y}z \bar{z}^3}{D}, \tag{D16}$$

where

$$D \equiv (\bar{z}^2 \bar{z}^4 - \bar{z}^3 \bar{z}^3). \tag{D17}$$

The corresponding squares of the standard deviations are

$$\sigma^2(\hat{\mu}_4)_{\text{stat}} = \frac{\bar{z}^4}{D}, \quad \sigma^2(\hat{\mu}_6)_{\text{stat}} = \frac{\bar{z}^2}{D}. \tag{D18}$$

When using Taylor expansion of $\chi^2(\mu_4, \mu_6)$ around the point $(\hat{\mu}_4, \hat{\mu}_6)$ up to the terms quadratic in the deviations, it can be checked that the following (approximate) relations hold:

$$\chi^2(\mu_4 = \hat{\mu}_4 \pm \sigma(\hat{\mu}_4)_{\text{stat}}, \mu_6 = \hat{\mu}_6) = \chi_{\text{min}}^2 + \frac{\bar{z}^2 \bar{z}^4}{D} \tag{D19a}$$

$$\chi^2(\mu_4 = \hat{\mu}_4, \mu_6 = \hat{\mu}_6 \pm \sigma(\hat{\mu}_6)_{\text{stat}}) = \chi_{\text{min}}^2 + \frac{\bar{z}^2 \bar{z}^4}{D} \tag{D19b}$$

We determined the values $\sigma(\hat{\mu}_4)_{\text{stat}}$ and $\sigma(\hat{\mu}_6)_{\text{stat}}$ from Eq. (D19).²⁰

²⁰ Equations (D19b) and (D18) give the same result for $\sigma(\hat{\mu}_6)_{\text{stat}}$. For $\sigma(\hat{\mu}_4)_{\text{stat}}$ [and $\sigma(\hat{f}_2)_{\text{stat}}$, cf. Eq. (D8)], the result of Eq. (D19a) differs from that of Eq. (D18) by a few percent ($\leq 5\%$), principally due to the effect of the running of $f_2^{p-n}(Q^2)$ with Q^2 .

Also the systematic uncertainties were estimated analogously to the case of $\mu_6 = 0$, cf. Sec. D.1, only the algebra is now more involved. The basis is again the identity (D10), but this time for the quantities $\overline{yz^2}$ and $\overline{y\bar{z}}$ which appear in $\hat{\mu}_4$ and $\hat{\mu}_6$, Eq. (D16) and can thus be expressed by $\hat{\mu}_4$ and $\hat{\mu}_6$

$$\overline{y\bar{z}} = \hat{\mu}_4 \overline{z^2} + \hat{\mu}_6 \overline{z^3}, \quad \overline{yz^2} = \hat{\mu}_4 \overline{z^3} + \hat{\mu}_6 \overline{z^4}. \tag{D20}$$

Using this, we obtain

$$\hat{\mu}_4 = \tilde{\mu}_4^{(1)} + \tilde{\mu}_4^{(2)}, \quad \hat{\mu}_6 = \tilde{\mu}_6^{(1)} + \tilde{\mu}_6^{(2)}, \tag{D21}$$

where

$$\begin{aligned} \tilde{\mu}_4^{(1)} &= \tilde{\alpha} \hat{\mu}_4^{(1)} - \kappa_{34} \hat{\mu}_6^{(1)}, \\ \tilde{\mu}_4^{(2)} &= (1 - \tilde{\alpha}) \hat{\mu}_4^{(2)} + \kappa_{34} \hat{\mu}_6^{(2)}, \end{aligned} \tag{D22a}$$

$$\begin{aligned} \tilde{\mu}_6^{(1)} &= \tilde{\beta} \hat{\mu}_6^{(1)} + \kappa_{23} \hat{\mu}_4^{(1)}, \\ \tilde{\mu}_6^{(2)} &= (1 - \tilde{\beta}) \hat{\mu}_6^{(2)} - \kappa_{23} \hat{\mu}_4^{(2)}. \end{aligned} \tag{D22b}$$

As earlier, we denote by ‘(1)’ and ‘(2)’ the experiments 1 (EG1b, [4]) and 2 (EG1-DVCS, [5]), and the constants appearing in Eq. (D22) are

$$\kappa_{34} = \frac{1}{D^{(1+2)}} \left(-\overline{z^3}^{(1)} \overline{z^4}^{(2)} + \overline{z^3}^{(2)} \overline{z^4}^{(1)} \right), \tag{D23a}$$

$$\kappa_{23} = \frac{1}{D^{(1+2)}} \left(-\overline{z^2}^{(1)} \overline{z^3}^{(2)} + \overline{z^2}^{(2)} \overline{z^3}^{(1)} \right), \tag{D23b}$$

$$\tilde{\alpha} = \frac{1}{D^{(1+2)}} \left(D^{(11)} + D^{(12)} \right), \tag{D23c}$$

$$\tilde{\beta} = \frac{1}{D^{(1+2)}} \left(D^{(11)} + D^{(21)} \right), \tag{D23d}$$

where the D -terms are defined as

$$D^{(ij)} = \frac{\overline{z^2}^{(i)} \overline{z^4}^{(j)}}{z^2 z^4} - \frac{\overline{z^3}^{(i)} \overline{z^3}^{(j)}}{z^3 z^3} \quad (i, j = 1, 2), \tag{D24a}$$

$$D^{(1+2)} = \sum_{j=1}^2 \sum_{i=1}^2 D^{(ij)} = \overline{z^2} \overline{z^4} - \overline{z^3} \overline{z^3}, \tag{D24b}$$

where in the last expression on the right-hand side, the unnormalized averages are made over the experiments 1 and 2.²¹

The estimates of the systematic uncertainties for the quantities $\tilde{\mu}_4^{(E)}$ and $\tilde{\mu}_6^{(E)}$, for experiments $E = 1, 2$, are evaluated in complete analogy with Eq. (D9) of the previous Sec. D2

$$\begin{aligned} (\delta \tilde{\mu}_N)_{sys}^{(E)} \equiv \sigma(\tilde{\mu}_N)_{sys}^{(E)} &\approx \frac{1}{2} \left(|\tilde{\mu}_N(UP)^{(E)} - \tilde{\mu}_N^{(E)}| \right. \\ &\quad \left. + |\tilde{\mu}_N(DO)^{(E)} - \tilde{\mu}_N^{(E)}| \right), \end{aligned} \tag{D25}$$

where $N = 4$ or $N = 6$. For explanations of the notation ‘UP’ and ‘DO’ we refer to the previous Sec.D.2. In our approxi-

²¹ This is somewhat different from the unnormalized averages \overline{A} appearing in Eqs. (D16)–(D18) which are over all the experimental points of the fit, i.e., over more than two experiments.

mation, we consider that the systematic uncertainties in the experiments 1 and 2 are mutually independent; this, in conjunction with the relations (D21), then gives

$$(\delta \hat{\mu}_4)_{sys} \equiv \sigma(\hat{\mu}_4)_{sys} = \left[\sigma^2(\tilde{\mu}_4^{(1)})_{sys} + \sigma^2(\tilde{\mu}_4^{(2)})_{sys} \right]^{1/2}, \tag{D26a}$$

$$(\delta \hat{\mu}_6)_{sys} \equiv \sigma(\hat{\mu}_6)_{sys} = \left[\sigma^2(\tilde{\mu}_6^{(1)})_{sys} + \sigma^2(\tilde{\mu}_6^{(2)})_{sys} \right]^{1/2}, \tag{D26b}$$

The systematic uncertainty of the extracted value f_2^{p-n} (1GeV²) is obtained then from Eq. (D26a) via the relation (6)

$$(\delta \hat{f}_2)_{sys} \equiv \sigma(\hat{f}_2)_{sys} = \frac{9}{4M_N^2} \sigma(\hat{\mu}_4)_{sys}. \tag{D27}$$

D.3 “Massive” OPE case

When the truncated OPE has, instead, a “massive” term Eq. (16), a similar estimation of the statistical and systematic uncertainties of the extracted parameters f_2^{p-n} (1GeV²) and M^2 can be made. This is so because, when expanding the “massive” higher-twist term in powers of $1/Q^2$, we obtain

$$\mu_6(M^2) = -M^2 \mu_4; \quad M^2 = -\frac{\mu_6}{\mu_4}. \tag{D28}$$

In the first approximation, the “massive” case can thus be considered as the case of truncated OPE (10). To estimate the statistical uncertainties of the extracted f_2^{p-n} (1GeV²) and M^2 , we decided to apply the relations of the type (D19)

$$\begin{aligned} \chi^2(\mu_4 = \hat{\mu}_4 \pm \sigma(\hat{\mu}_4)_{stat}, M^2 = \hat{M}^2) \\ = \chi_{min}^2 + \frac{\overline{z^2} \overline{z^4}}{D} \end{aligned} \tag{D29a}$$

$$\begin{aligned} \chi^2(\mu_4 = \hat{\mu}_4, M^2 = \hat{M}^2 \pm \sigma(\hat{M}^2)_{stat}) \\ = \chi_{min}^2 + \frac{\overline{z^2} \overline{z^4}}{D}. \end{aligned} \tag{D29b}$$

To estimate the systematic uncertainties in the “massive” case, the relations (D26) for μ_4 and μ_6 were used. Namely, differentiation of the relation (D28) gives an approximate relation

$$\begin{aligned} \sigma^2(M^2)_{sys} \approx \left(\frac{\hat{\mu}_6}{\hat{\mu}_4^2} \right)^2 \sigma^2(\hat{\mu}_4)_{sys} + \frac{1}{\hat{\mu}_4^2} \sigma^2(\hat{\mu}_6)_{sys} \\ - 2 \left(\frac{\hat{\mu}_6}{\hat{\mu}_4^3} \right) \langle \delta \hat{\mu}_4 \delta \hat{\mu}_6 \rangle_{sys}, \end{aligned} \tag{D30}$$

where in the first two terms on the right-hand side we can use the expressions (D26), and in the last term the correlator $\langle \delta \hat{\mu}_4 \delta \hat{\mu}_6 \rangle_{sys}$ can be estimated in a similar way as other correlators described above. Motivated by the relations (D21), we chose the following estimate for this correlator:

$$\begin{aligned} & \langle \delta \hat{\mu}_4 \delta \hat{\mu}_6 \rangle_{\text{sys}} \\ &= \frac{1}{2} \sum_{E=1}^2 \left[\left(\tilde{\mu}_4^{(E)}(UP) - \tilde{\mu}_4^{(E)} \right) \left(\tilde{\mu}_6^{(E)}(UP) - \tilde{\mu}_6^{(E)} \right) \right. \\ & \quad \left. + \left(\tilde{\mu}_4^{(E)}(DO) - \tilde{\mu}_4^{(E)} \right) \left(\tilde{\mu}_6^{(E)}(DO) - \tilde{\mu}_6^{(E)} \right) \right]. \quad (\text{D31}) \end{aligned}$$

We note that in the ‘‘massive’’ case the systematic uncertainties are often quite large, so the estimate (D30) should be regarded often as only a rough approximation.

Appendix E: Charm mass effects in BSR

The contributions of the finite charm quark mass, i.e., the effects beyond $N_f = 3$, in the polarized BSR at NLO were evaluated in [136]. When ignoring the b -quark contributions (considering $m_b \rightarrow \infty$), the mentioned effects at NLO can be expressed with the function $C_{\text{pBJ}}^{\text{mass.},(2)}(\xi_c)$, where $\xi_c \equiv Q^2/m_c^2$ which is assumed in [136] to be $\xi_c \gtrsim 1$, and $m_c \approx 1.59 \text{ GeV}$ is the pole mass. This function appears in the NLO coefficient (at a^2) when the perturbation expansion (4) is reexpressed in terms of the $N_f = 4$ coupling $a_{N_f=4}$

$$\begin{aligned} \mathcal{D}_{\text{BS}}(Q^2)_{\text{pt}} = & a(Q^2)_{N_f=4} + a(Q^2)_{N_f=4}^2 \left\{ \frac{55}{12} - \frac{1}{3} \left[N_f - 1 \right. \right. \\ & \left. \left. + C_{\text{pBJ}}^{\text{mass.},(2)}(\xi_c) \right] \right\} + \mathcal{O}(a^3), \quad (\text{E1}) \end{aligned}$$

where $N_f = 4$ and

$$\begin{aligned} C_{\text{pBJ}}^{\text{mass.},(2)}(\xi) = & \frac{1}{2520} \left\{ \frac{1}{\xi} (6\xi^2 + 2735\xi + 11724) \right. \\ & - \frac{\sqrt{\xi+4}}{\xi^{3/2}} (3\xi^3 + 106\xi^2 + 1054\xi + 4812) \\ & \times \ln \left[\frac{\sqrt{\xi+4} + \sqrt{\xi}}{\sqrt{\xi+4} - \sqrt{\xi}} \right] \\ & - 2100 \frac{1}{\xi^2} \ln^2 \left[\frac{\sqrt{\xi+4} + \sqrt{\xi}}{\sqrt{\xi+4} - \sqrt{\xi}} \right] \\ & \left. + (3\xi^2 + 112\xi + 1260) \ln \xi \right\} \quad (\xi \gtrsim 1). \quad (\text{E2}) \end{aligned}$$

When $Q^2 \gg m_c^2$ ($\xi \gg 1$), this function approaches unity quite slowly

$$C_{\text{pBJ}}^{\text{mass.},(2)}(\xi) = 1 - \frac{8 \ln \xi}{3 \xi} + \frac{34}{9\xi} + \mathcal{O}\left(\frac{\ln^2 \xi}{\xi^2}\right). \quad (\text{E3})$$

In this limit ($\xi_c \rightarrow \infty$) this then gives in the expansion (E1) the massless expression for the NLO coefficient $d_1(N_f)$ with $N_f = 4$

$$d_1(N_f) = \frac{55}{12} - \frac{1}{3} N_f. \quad (\text{E4})$$

As noted, the convergence to the $N_f = 4$ case (four massless quarks) is rather slow in BSR. Specifically, 3 +

$C_{\text{pBJ}}^{\text{mass.},(2)}(Q^2/m_c^2) \approx 3.13, 3.36, 3.73, 3.83$ for $Q^2 = 5, 10, 50, 100 \text{ GeV}^2$, respectively. This indicates that at $Q^2 = 5 \text{ GeV}^2$ (the highest considered experimental Q^2 in BSR) we are still rather far away from the $N_f = 4$ case. Therefore, it appears reasonable to use $N_f = 3$ (i.e., decoupled charm quark) in the polarized BSR for the interval $0 < Q^2 < 5 \text{ GeV}^2$ considered in the present work.

References

- J.D. Bjorken, Applications of the chiral $U(6) \times (6)$ algebra of current densities. Phys. Rev. **148**, 1467 (1966)
- J.D. Bjorken, Inelastic scattering of polarized leptons from polarized nucleons. Phys. Rev. D **1**, 1376 (1970)
- A. Deur et al., Experimental determination of the evolution of the Bjorken integral at low Q^2 . Phys. Rev. Lett. **93**, 212001 (2004). [arXiv:hep-ex/0407007](https://arxiv.org/abs/hep-ex/0407007)
- A. Deur, Experimental study of isovector spin sum rules. Phys. Rev. D **78**, 032001 (2008). [arXiv:0802.3198](https://arxiv.org/abs/0802.3198) [nucl-ex]
- A. Deur et al., High precision determination of the Q^2 evolution of the Bjorken Sum. Phys. Rev. D **90**, 012009 (2014). [arXiv:1405.7854](https://arxiv.org/abs/1405.7854) [nucl-ex]
- C. Adolph et al. (COMPASS Collaboration), The spin structure function g_1^p of the proton and a test of the Bjorken sum rule. Phys. Lett. B **753**, 18 (2016). [arXiv:1503.08935](https://arxiv.org/abs/1503.08935) [hep-ex]
- C. Adolph et al. (COMPASS Collaboration), Final COMPASS results on the deuteron spin-dependent structure function g_1^d and the Bjorken sum rule. Phys. Lett. B **769**, 34 (2017). [arXiv:1612.00620](https://arxiv.org/abs/1612.00620) [hep-ex]
- K. Abe et al. (E143 Collaboration), Measurements of the proton and deuteron spin structure functions g_1 and g_2 . Phys. Rev. D **58**, 112003 (1998). [arXiv:hep-ph/9802357](https://arxiv.org/abs/hep-ph/9802357)
- P.L. Anthony et al. (E155 Collaboration), Measurements of the Q^2 dependence of the proton and neutron spin structure functions g_1^p and g_1^n . Phys. Lett. B **493**, 19 (2000). [arXiv:hep-ph/0007248](https://arxiv.org/abs/hep-ph/0007248)
- D. Adams et al. (Spin Muon (SMC) Collaboration), Spin structure of the proton from polarized inclusive deep inelastic muon-proton scattering. Phys. Rev. D **56**, 5330 (1997). [arXiv:hep-ex/9702005](https://arxiv.org/abs/hep-ex/9702005)
- A. Airapetian et al. (HERMES Collaboration), Precise determination of the spin structure function g_1 of the proton, deuteron and neutron. Phys. Rev. D **75**, 012007 (2007). [arXiv:hep-ex/0609039](https://arxiv.org/abs/hep-ex/0609039)
- Y. Prok et al. (CLAS Collaboration), Precision measurements of g_1 of the proton and the deuteron with 6 GeV electrons. Phys. Rev. C **90**(2), 025212 (2014). [arXiv:1404.6231](https://arxiv.org/abs/1404.6231) [nucl-ex]
- D.V. Shirkov, I.L. Solovtsov, Analytic QCD running coupling with finite IR behaviour and universal $\bar{\alpha}_s(0)$ value. JINR Rapid Commun. **2**(76), 5–10 (1996). [arXiv:hep-ph/9604363](https://arxiv.org/abs/hep-ph/9604363)
- D.V. Shirkov, I.L. Solovtsov, Analytic model for the QCD running coupling with universal $\alpha_s(0)$ value. Phys. Rev. Lett. **79**, 1209 (1997). [arXiv:hep-ph/9704333](https://arxiv.org/abs/hep-ph/9704333)
- K.A. Milton, I.L. Solovtsov, Analytic perturbation theory in QCD and Schwinger’s connection between the beta function and the spectral density. Phys. Rev. D **55**, 5295 (1997). [arXiv:hep-ph/9611438](https://arxiv.org/abs/hep-ph/9611438)
- I.L. Solovtsov, D.V. Shirkov, Analytic approach to perturbative QCD and renormalization scheme dependence. Phys. Lett. B **442**, 344 (1998). [arXiv:hep-ph/9711251](https://arxiv.org/abs/hep-ph/9711251)
- D.V. Shirkov, Analytic perturbation theory for QCD observables. Theor. Math. Phys. **127**, 409 (2001). [arXiv:hep-ph/0012283](https://arxiv.org/abs/hep-ph/0012283)
- D.V. Shirkov, Analytic perturbation theory in analyzing some QCD observables. Eur. Phys. J. C **22**, 331 (2001). [arXiv:hep-ph/0107282](https://arxiv.org/abs/hep-ph/0107282)

19. A.P. Bakulev, S.V. Mikhailov, N.G. Stefanis, QCD analytic perturbation theory: from integer powers to any power of the running coupling. *Phys. Rev. D* **72**, 074014 (2005). [arXiv:hep-ph/0506311](#) [*Phys. Rev. D* **72**, 119908(E) (2005)]
20. A.P. Bakulev, A.I. Karanikas, N.G. Stefanis, Analyticity properties of three-point functions in QCD beyond leading order. *Phys. Rev. D* **72**, 074015 (2005). [arXiv:hep-ph/0504275](#)
21. A.P. Bakulev, S.V. Mikhailov, N.G. Stefanis, Fractional Analytic Perturbation Theory in Minkowski space and application to Higgs boson decay into a $b\bar{b}$ pair. *Phys. Rev. D* **75**, 056005 (2007). <https://doi.org/10.1103/PhysRevD.75.056005>. [arXiv:hep-ph/0607040](#) [Erratum: *Phys. Rev. D* **77**, 079901 (2008)]
22. A.P. Bakulev, S.V. Mikhailov, N.G. Stefanis, *Phys. Rev. D* **77**, 079901(E) (2008). [arXiv:hep-ph/0607040](#)
23. A.P. Bakulev, S.V. Mikhailov, N.G. Stefanis, Higher-order QCD perturbation theory in different schemes: from FOPT to CIPT to FAPT. *JHEP* **1006**, 085 (2010). [arXiv:1004.4125](#) [hep-ph]
24. G.M. Prospero, M. Raciti, C. Simolo, On the running coupling constant in QCD. *Prog. Part. Nucl. Phys.* **58**, 387 (2007). [arXiv:hep-ph/0607209](#)
25. D.V. Shirkov, I.L. Solovtsov, Ten years of the analytic perturbation theory in QCD. *Theor. Math. Phys.* **150**, 132 (2007). [arXiv:hep-ph/0611229](#)
26. A.P. Bakulev, Global fractional analytic perturbation theory in QCD with selected applications. *Phys. Part. Nucl.* **40**, 715 (2009). [arXiv:0805.0829](#) [hep-ph] (arXiv preprint in Russian)
27. N.G. Stefanis, Taming Landau singularities in QCD perturbation theory: the analytic approach. *Phys. Part. Nucl.* **44**, 494 (2013). [arXiv:0902.4805](#) [hep-ph]
28. R.S. Pasechnik, D.V. Shirkov, O.V. Teryaev, Bjorken sum rule and pQCD frontier on the move. *Phys. Rev. D* **78**, 071902 (2008). [arXiv:0808.0066](#) [hep-ph]
29. R.S. Pasechnik, D.V. Shirkov, O.V. Teryaev, O.P. Solovtsova, V.L. Khandramai, Nucleon spin structure and pQCD frontier on the move. *Phys. Rev. D* **81**, 016010 (2010). [arXiv:0911.3297](#) [hep-ph]
30. V.L. Khandramai, R.S. Pasechnik, D.V. Shirkov, O.P. Solovtsova, O.V. Teryaev, Four-loop QCD analysis of the Bjorken sum rule vs data. *Phys. Lett. B* **706**, 340 (2012). [arXiv:1106.6352](#) [hep-ph]
31. V.L. Khandramai, O.P. Solovtsova, O.V. Teryaev, Polarized Bjorken sum rule analysis: revised. *Nonlinear Phenom. Complex Syst.* **16**, 93 (2013). [arXiv:1302.3952](#) [hep-ph]
32. C. Ayala, C. Contreras, G. Cvetič, Extended analytic QCD model with perturbative QCD behavior at high momenta. *Phys. Rev. D* **85**, 114043 (2012). [arXiv:1203.6897](#) [hep-ph]; in Eqs. (21) and (22) of this reference there is a typo: the lower limit of integration is written as $s_L - \eta$; it is in fact $-s_L - \eta$
33. C. Ayala, G. Cvetič, anQCD: a Mathematica package for calculations in general analytic QCD models. *Comput. Phys. Commun.* **190**, 182 (2015). [arXiv:1408.6868](#) [hep-ph]
34. C. Ayala, G. Cvetič, R. Kögerler, Lattice-motivated holomorphic nearly perturbative QCD. *J. Phys. G* **44**(7), 075001 (2017). [arXiv:1608.08240](#) [hep-ph]
35. C. Ayala, G. Cvetič, R. Kögerler, I. Kondrashuk, Nearly perturbative lattice-motivated QCD coupling with zero IR limit. *J. Phys. G* **45**(3), 035001 (2018). [arXiv:1703.01321](#) [hep-ph]
36. C. Ayala, G. Cvetič, A.V. Kotikov, B.G. Shaikhmatdenov, Bjorken sum rule in QCD frameworks with analytic (holomorphic) coupling. *Int. J. Mod. Phys. A* **33**(18n19), 1850112 (2018). [arXiv:1708.06284](#) [hep-ph]
37. C. Ayala, G. Cvetič, A.V. Kotikov, B.G. Shaikhmatdenov, Bjorken sum rule in QCD with analytic coupling. *J. Phys. Conf. Ser.* **938**(1), 012055 (2017). [arXiv:1712.06048](#) [hep-ph]
38. A. Deur, S.J. Brodsky, G.F. de Teramond, The QCD running coupling. *Prog. Part. Nucl. Phys.* **90**, 1 (2016). [arXiv:1604.08082](#) [hep-ph]
39. C. Patrignani et al. (Particle Data Group Collaboration), Review of particle physics. *Chin. Phys. C* **40**(10), 100001 (2016)
40. S.G. Gorishnii, S.A. Larin, QCD corrections to the parton model rules for structure functions of deep inelastic scattering. *Phys. Lett. B* **172**, 109 (1986)
41. S.A. Larin, J.A.M. Vermaseren, The α_s^3 corrections to the Bjorken sum rule for polarized electroproduction and to the Gross-Llewellyn Smith sum rule. *Phys. Lett. B* **259**, 345 (1991)
42. P.A. Baikov, K.G. Chetyrkin, J.H. Kühn, Adler function, Bjorken sum rule, and the Crewther relation to order α_s^4 in a general gauge theory. *Phys. Rev. Lett.* **104**, 132004 (2010). [arXiv:1001.3606](#) [hep-ph]
43. P.A. Baikov, K.G. Chetyrkin, J.H. Kühn, Massless propagators, $R(s)$ and multiloop QCD. *Nucl. Part. Phys. Proc.* **261–262**, 3 (2015). <https://doi.org/10.1016/j.nuclphysbps.2015.03.002>. [arXiv:1501.06739](#) [hep-ph]
44. S.A. Larin, The singlet contribution to the Bjorken sum rule for polarized deep inelastic scattering. *Phys. Lett. B* **723**, 348 (2013). [arXiv:1303.4021](#) [hep-ph]
45. G. Cvetič, C. Valenzuela, An approach for evaluation of observables in analytic versions of QCD. *J. Phys. G* **32**, L27 (2006). [arXiv:hep-ph/0601050](#)
46. G. Cvetič, C. Valenzuela, Various versions of analytic QCD and skeleton-motivated evaluation of observables. *Phys. Rev. D* **74**, 114030 (2006). [arXiv:hep-ph/0608256](#) [Erratum-ibid. *D* **84**, 019902 (2011)]
47. G. Cvetič, A.V. Kotikov, Analogs of noninteger powers in general analytic QCD. *J. Phys. G* **39**, 065005 (2012). [arXiv:1106.4275](#) [hep-ph]
48. E.V. Shuryak, A.I. Vainshtein, Theory of power corrections to deep inelastic scattering in quantum chromodynamics. 2. Q^4 effects: polarized target. *Nucl. Phys. B* **201**, 141 (1982)
49. H. Kawamura, T. Uematsu, J. Kodaira, Y. Yasui, Renormalization of twist four operators in QCD Bjorken and Ellis–Jaffe sum rules. *Mod. Phys. Lett. A* **12**, 135 (1997). [arXiv:hep-ph/9603338](#)
50. A.L. Kataev, A.V. Kotikov, G. Parente, A.V. Sidorov, Next to next-to-leading order QCD analysis of the revised CCFR data for $x F_3$ structure function and the higher twist contributions. *Phys. Lett. B* **417**, 374 (1998). [arXiv:hep-ph/9706534](#)
51. A.L. Kataev, G. Parente, A.V. Sidorov, Higher twists and $\alpha_s(M_Z)$ extractions from the NNLO QCD analysis of the CCFR data for the $x F_3$ structure function. *Nucl. Phys. B* **573**, 405 (2000). [arXiv:hep-ph/9905310](#)
52. A.L. Kataev, G. Parente, A.V. Sidorov, Improved fits to the $x F_3$ CCFR data at the next-to-next-to-leading order and beyond. *Phys. Part. Nucl.* **34**, 20 (2003). [arXiv:hep-ph/0106221](#) [*Fiz. Elem. Chast. Atom. Yadra* **34**, 43 (2003)] Erratum: [*Phys. Part. Nucl.* **38**(6), 827 (2007)]
53. S. Narison, V.I. Zakharov, Duality between QCD perturbative series and power corrections. *Phys. Lett. B* **679**, 355 (2009). [arXiv:0906.4312](#) [hep-ph]
54. G. Parente, A.V. Kotikov, V.G. Krivokhizhin, Next to next-to-leading order QCD analysis of DIS structure functions. *Phys. Lett. B* **333**, 190 (1994). [arXiv:hep-ph/9405290](#)
55. B.G. Shaikhmatdenov, A.V. Kotikov, V.G. Krivokhizhin, G. Parente, QCD coupling constant at NNLO from DIS data. *Phys. Rev. D* **81**, 034008 (2010). [arXiv:0912.4672](#) [hep-ph] [Erratum: *Phys. Rev. D* **81**, 079904 (2010)]
56. A.V. Kotikov, V.G. Krivokhizhin, B.G. Shaikhmatdenov, Analytic and ‘frozen’ QCD coupling constants up to NNLO from DIS data. *Phys. Atom. Nucl.* **75**, 507 (2012). [arXiv:1008.0545](#) [hep-ph]

57. A.V. Kotikov, V.G. Krivokhizhin, B.G. Shaikhatdenov, Improved nonsinglet QCD analysis of fixed-target DIS data. *J. Phys. G* **42**(9), 095004 (2015). [arXiv:1411.1236](https://arxiv.org/abs/1411.1236) [hep-ph]
58. S. Simula, M. Osipenko, G. Ricco, M. Taiuti, Leading and higher twists in the proton polarized structure function g_1^p at large Bjorken x . *Phys. Rev. D* **65**, 034017 (2002). [arXiv:hep-ph/0107036](https://arxiv.org/abs/hep-ph/0107036)
59. P. Mergell, U.G. Meissner, D. Drechsel, Dispersion theoretical analysis of the nucleon electromagnetic form-factors. *Nucl. Phys. A* **596**, 367 (1996). [arXiv:hep-ph/9506375](https://arxiv.org/abs/hep-ph/9506375)
60. R.S. Sufian, G.F. de Téramond, S.J. Brodsky, A. Deur, H.G. Dosch, Analysis of nucleon electromagnetic form factors from light-front holographic QCD: the spacelike region. *Phys. Rev. D* **95**(1), 014011 (2017). [arXiv:1609.06688](https://arxiv.org/abs/1609.06688) [hep-ph]
61. K.A. Olive et al. (Particle Data Group Collaboration), Review of particle physics. *Chin. Phys. C* **38**, 090001 (2014)
62. A.V. Kotikov, G. Parente, J. Sánchez Guillén, Renormalization scheme invariant analysis of the DIS structure functions F_2 and F_L . *Z. Phys. C* **58**, 465 (1993)
63. V.G. Krivokhizhin, A.V. Kotikov, A systematic study of QCD coupling constant from deep-inelastic measurements. *Phys. Atom. Nucl.* **68**, 1873 (2005) [*Yad. Fiz.* **68**, 1935 (2005)]
64. A.V. Kotikov, A.V. Lipatov, N.P. Zotov, The longitudinal structure function F_L : perturbative QCD and k_T factorization versus experimental data at fixed W . *J. Exp. Theor. Phys.* **101**, 811 (2005)
65. A.V. Kotikov, A.V. Lipatov, N.P. Zotov, The longitudinal structure function F_L : perturbative QCD and k_T factorization versus experimental data at fixed W . *Zh. Eksp. Teor. Fiz.* **128**, 938 (2005). [arXiv:hep-ph/0403135](https://arxiv.org/abs/hep-ph/0403135)
66. A.Y. Illarionov, A.V. Kotikov, G. Parente Bermudez, Small x behavior of parton distributions. A Study of higher twist effects. *Phys. Part. Nucl.* **39**, 307 (2008). [arXiv:hep-ph/0402173](https://arxiv.org/abs/hep-ph/0402173)
67. G. Cvetič, A.Y. Illarionov, B.A. Kniehl, A.V. Kotikov, Small- x behavior of the structure function F_2 and its slope $\partial \ln F_2 / \partial \ln(1/x)$ for ‘frozen’ and analytic strong-coupling constants. *Phys. Lett. B* **679**, 350 (2009). [arXiv:0906.1925](https://arxiv.org/abs/0906.1925) [hep-ph]
68. A.V. Kotikov, B.G. Shaikhatdenov, Q^2 -evolution of parton densities at small x values. Combined H1 and ZEUS F_2 data. *Phys. Part. Nucl.* **44**, 543 (2013). [arXiv:1212.4582](https://arxiv.org/abs/1212.4582) [hep-ph]
69. A.V. Kotikov, B.G. Shaikhatdenov, Q^2 evolution of parton distributions at small values of x : effective scale for combined H1 and ZEUS data on the structure function F_2 . *Phys. Atom. Nucl.* **78**(4), 525 (2015). [arXiv:1402.4349](https://arxiv.org/abs/1402.4349) [hep-ph]
70. A.V. Kotikov, B.G. Shaikhatdenov, Q^2 -evolution of parton densities at small x values. Charm contribution in the combined H1 and ZEUS F_2 data. *Phys. Part. Nucl.* **48**(5), 829 (2017). [arXiv:1606.07888](https://arxiv.org/abs/1606.07888) [hep-ph]
71. F.D. Aaron et al. (H1 and ZEUS Collaborations), Combined measurement and QCD analysis of the inclusive $e^\pm p$ scattering cross sections at HERA. *JHEP* **1001**, 109 (2010). [arXiv:0911.0884](https://arxiv.org/abs/0911.0884) [hep-ex]
72. I.L. Bogolubsky, E.-M. Ilgenfritz, M. Müller-Preussker, A. Sternbeck, Lattice gluodynamics computation of Landau gauge Green’s functions in the deep infrared. *Phys. Lett. B* **676**, 69 (2009). [arXiv:0901.0736](https://arxiv.org/abs/0901.0736) [hep-lat]
73. A.G. Duarte, O. Oliveira, P.J. Silva, Lattice gluon and ghost propagators, and the strong coupling in pure SU(3) Yang–Mills theory: finite lattice spacing and volume effects. *Phys. Rev. D* **94**(1), 014502 (2016). [arXiv:1605.00594](https://arxiv.org/abs/1605.00594) [hep-lat]
74. E.-M. Ilgenfritz, M. Müller-Preussker, A. Sternbeck, A. Schiller, Gauge-variant propagators and the running coupling from lattice QCD. [arXiv:hep-lat/0601027](https://arxiv.org/abs/hep-lat/0601027)
75. B. Blossier et al., The strong running coupling at τ and Z_0 mass scales from lattice QCD. *Phys. Rev. Lett.* **108**, 262002 (2012). [arXiv:1201.5770](https://arxiv.org/abs/1201.5770) [hep-ph]
76. B. Blossier et al., Ghost-gluon coupling, power corrections and $\Lambda_{\overline{\text{MS}}}$ from lattice QCD with a dynamical charm. *Phys. Rev. D* **85**, 034503 (2012). [arXiv:1110.5829](https://arxiv.org/abs/1110.5829) [hep-lat]
77. O. Teryaev, Analyticity and higher twists. *Nucl. Phys. Proc. Suppl.* **245**, 195 (2013). [arXiv:1309.1985](https://arxiv.org/abs/1309.1985) [hep-ph]
78. V.L. Khandramai, O.V. Teryaev, I.R. Gabdrakhmanov, Infrared modified QCD couplings and Bjorken sum rule. *J. Phys. Conf. Ser.* **678**(1), 012018 (2016)
79. I.R. Gabdrakhmanov, O.V. Teryaev, V.L. Khandramai, Infrared models for the Bjorken sum rule in the APT approach. *J. Phys. Conf. Ser.* **938**(1), 012046 (2017)
80. D.V. Shirkov, ‘Massive’ perturbative QCD, regular in the IR limit. *Phys. Part. Nucl. Lett.* **10**, 186 (2013). [arXiv:1208.2103](https://arxiv.org/abs/1208.2103) [hep-th]
81. D.V. Shirkov, Remarks on simple modified perturbation theory. *Phys. Part. Nucl. Lett.* **12**(2), 205 (2015)
82. J.M. Cornwall, Dynamical mass generation in continuum QCD. *Phys. Rev. D* **26**, 1453 (1982)
83. A.C. Aguilar, D. Binosi, J. Papavassiliou, Renormalization group analysis of the gluon mass equation. *Phys. Rev. D* **89**(8), 085032 (2014). [arXiv:1401.3631](https://arxiv.org/abs/1401.3631) [hep-ph]
84. S.B. Gerasimov, A sum rule for magnetic moments and the damping of the nucleon magnetic moment in nuclei. *Sov. J. Nucl. Phys.* **2**, 430 (1966) [*Yad. Fiz.* **2**, 598 (1965)]
85. M. Anselmino, B.L. Ioffe, E. Leader, On possible resolutions of the spin crisis in the parton model. *Sov. J. Nucl. Phys.* **49**, 136 (1989); [*Yad. Fiz.* **49**, 214 (1989)]
86. J. Soffer, O. Teryaev, The role of $g-2$ in relating the Schwinger and Gerasimov–Drell–Hearn sum rules. *Phys. Rev. Lett.* **70**, 3373 (1993). <https://doi.org/10.1103/PhysRevLett.70.3373>
87. J. Soffer, O.V. Teryaev, On the G_2 manifestation for longitudinally polarized particles. *Phys. Rev. D* **51**, 25 (1995). <https://doi.org/10.1103/PhysRevD.51.25>. [arXiv:hep-ph/9405228](https://arxiv.org/abs/hep-ph/9405228)
88. J. Soffer, O. Teryaev, QCD radiative and power corrections and generalized GDH sum rules. *Phys. Rev. D* **70**, 116004 (2004). <https://doi.org/10.1103/PhysRevD.70.116004>. [arXiv:hep-ph/0410228](https://arxiv.org/abs/hep-ph/0410228)
89. J. Soffer, O. Teryaev, *Phys. Rev. D* **70**, 116004 (2004). [arXiv:hep-ph/0410228](https://arxiv.org/abs/hep-ph/0410228)
90. S.J. Brodsky, G.F. de Téramond, A. Deur, Nonperturbative QCD coupling and its β -function from light-front holography. *Phys. Rev. D* **81**, 096010 (2010). [arXiv:1002.3948](https://arxiv.org/abs/1002.3948) [hep-ph]
91. A. Deur, J.M. Shen, X.G. Wu, S.J. Brodsky, G.F. de Téramond, Implications of the principle of maximum conformality for the QCD strong coupling. *Phys. Lett. B* **773**, 98 (2017). [arXiv:1705.02384](https://arxiv.org/abs/1705.02384) [hep-ph]
92. A. Deur, S.J. Brodsky, G.F. de Téramond, Determination of $\Lambda_{\overline{\text{MS}}}$ at five loops from holographic QCD. *J. Phys. G* **44**(10), 105005 (2017). [arXiv:1608.04933](https://arxiv.org/abs/1608.04933) [hep-ph]
93. V.D. Burkert, Comment on the generalized Gerasimov–Drell–Hearn sum rule in chiral perturbation theory. *Phys. Rev. D* **63**, 097904 (2001). [arXiv:nucl-th/0004001](https://arxiv.org/abs/nucl-th/0004001)
94. V. Bernard, E. Epelbaum, H. Krebs, U.G. Meissner, New insights into the spin structure of the nucleon. *Phys. Rev. D* **87**(5), 054032 (2013). [arXiv:1209.2523](https://arxiv.org/abs/1209.2523) [hep-ph]
95. V. Lensky, J.M. Alarcón, V. Pascalutsa, Moments of nucleon structure functions at next-to-leading order in baryon chiral perturbation theory. *Phys. Rev. C* **90**(5), 055202 (2014). [arXiv:1407.2574](https://arxiv.org/abs/1407.2574) [hep-ph]
96. G. Cvetič, C. Villavicencio, Operator product expansion with analytic QCD in tau decay physics. *Phys. Rev. D* **86**, 116001 (2012). [arXiv:1209.2953](https://arxiv.org/abs/1209.2953) [hep-ph]
97. P.M. Stevenson, Optimized perturbation theory. *Phys. Rev. D* **23**, 2916 (1981)
98. G. Cvetič, R. Kögerler, Scale and scheme independent extension of Padé approximants: Bjorken polarized sum rule as an example. *Phys. Rev. D* **63**, 056013 (2001). [arXiv:hep-ph/0006098](https://arxiv.org/abs/hep-ph/0006098)

99. G. Cvetič, Techniques of evaluation of QCD low-energy physical quantities with running coupling with infrared fixed point. Phys. Rev. D **89**(3), 036003 (2014). [arXiv:1309.1696](#) [hep-ph]
100. A.V. Nesterenko, C. Simolo, QCDMAPT: program package for analytic approach to QCD. Comput. Phys. Commun. **181**, 1769 (2010). [arXiv:1001.0901](#) [hep-ph]
101. A.V. Nesterenko, C. Simolo, QCDMAPT_F: Fortran version of QCDMAPT package. Comput. Phys. Commun. **182**, 2303 (2011). [arXiv:1107.1045](#) [hep-ph]
102. C. Ayala, G. Cvetič, anQCD: Fortran programs for couplings at complex momenta in various analytic QCD models. Comput. Phys. Commun. **199**, 114 (2016). [arXiv:1506.07201](#) [hep-ph]
103. A.P. Bakulev, V.L. Khandramai, FAPT: a mathematica package for calculations in QCD fractional analytic perturbation theory. Comput. Phys. Commun. **184**(1), 183 (2013). [arXiv:1204.2679](#) [hep-ph]
104. G.A. Baker, P. Graves-Morris, *Padé Approximants. Encyclopedia of Mathematics and Its Applications* (Cambridge University Press, Cambridge 1996) (Section 5.4, Theorem 5.4.2)
105. S. Peris, Large- N_c QCD and Padé approximant theory. Phys. Rev. D **74**, 054013 (2006). [arXiv:hep-ph/0603190](#)
106. K.G. Chetyrkin, B.A. Kniehl, M. Steinhauser, Strong coupling constant with flavour thresholds at four loops in the MS-bar scheme. Phys. Rev. Lett. **79**, 2184 (1997). [arXiv:hep-ph/9706430](#)
107. A.C. Aguilar, J. Papavassiliou, Power-law running of the effective gluon mass. Eur. Phys. J. A **35**, 189 (2008). [arXiv:0708.4320](#) [hep-ph]
108. A.C. Aguilar, D. Binosi, J. Papavassiliou, J. Rodríguez-Quintero, Non-perturbative comparison of QCD effective charges. Phys. Rev. D **80**, 085018 (2009). [arXiv:0906.2633](#) [hep-ph]
109. D. Binosi, C. Mezrag, J. Papavassiliou, C.D. Roberts, J. Rodríguez-Quintero, Process-independent strong running coupling. Phys. Rev. D **96**(5), 054026 (2017). [arXiv:1612.04835](#) [nucl-th]
110. L. von Smekal, K. Maltman, A. Sternbeck, The strong coupling and its running to four loops in a minimal MOM scheme. Phys. Lett. B **681**, 336 (2009). [arXiv:0903.1696](#) [hep-ph]
111. P. Boucaud, F. De Soto, J.P. Leroy, A. Le Yaouanc, J. Micheli, O. Pene, J. Rodríguez-Quintero, Ghost-gluon running coupling, power corrections and the determination of Lambda(MS-bar). Phys. Rev. D **79**, 014508 (2009). [arXiv:0811.2059](#) [hep-ph]
112. K.G. Chetyrkin, A. Retey, Three loop three linear vertices and four loop similar to MOM beta functions in massless QCD. [arXiv:hep-ph/0007088](#)
113. A.L. Kataev, V.S. Molokoedov, Fourth-order QCD renormalization group quantities in the V scheme and the relation of the β function to the Gell-Mann–Low function in QED. Phys. Rev. D **92**, 054008 (2015). [arXiv:1507.03547](#) [hep-ph]
114. A.V. Garkusha, A.L. Kataev, V.S. Molokoedov, Renormalization scheme and gauge (in)dependence of the generalized Crewther relation: what are the real grounds of the β -factorization property? JHEP **1802**, 161 (2018). [arXiv:1801.06231](#) [hep-ph]
115. B.A. Arbuzov, I.V. Zaitsev, Elimination of the Landau pole in QCD with the spontaneously generated anomalous three-gluon interaction. [arXiv:1303.0622](#) [hep-th]
116. P. Boucaud, F. De Soto, A. Le Yaouanc, J.P. Leroy, J. Micheli, H. Moutarde, O. Pene, J. Rodríguez-Quintero, The strong coupling constant at small momentum as an instanton detector. JHEP **0304**, 005 (2003). [arXiv:hep-ph/0212192](#)
117. P. Boucaud, F. De Soto, A. Le Yaouanc, J.P. Leroy, J. Micheli, O. Pene, J. Rodríguez-Quintero, Modified instanton profile effects from lattice Green functions. Phys. Rev. D **70**, 114503 (2004). [arXiv:hep-ph/0312332](#)
118. M. Baldicchi, A.V. Nesterenko, G.M. Prosperi, D.V. Shirkov, C. Simolo, Bound state approach to the QCD coupling at low energy scales. Phys. Rev. Lett. **99**, 242001 (2007). [arXiv:0705.0329](#) [hep-ph]
119. M. Baldicchi, A.V. Nesterenko, G.M. Prosperi, C. Simolo, QCD coupling below 1 GeV from quarkonium spectrum. Phys. Rev. D **77**, 034013 (2008). [arXiv:0705.1695](#) [hep-ph]
120. G. Cvetič, C. Valenzuela, Analytic QCD: a short review. Braz. J. Phys. **38**, 371 (2008). [arXiv:0804.0872](#) [hep-ph]
121. A.V. Nesterenko, Quark antiquark potential in the analytic approach to QCD. Phys. Rev. D **62**, 094028 (2000). [arXiv:hep-ph/9912351](#)
122. A.V. Nesterenko, New analytic running coupling in space-like and timelike regions. Phys. Rev. D **64**, 116009 (2001). [arXiv:hep-ph/0102124](#)
123. A.V. Nesterenko, Analytic invariant charge in QCD. Int. J. Mod. Phys. A **18**, 5475 (2003). [arXiv:hep-ph/0308288](#)
124. A.C. Aguilar, A.V. Nesterenko, J. Papavassiliou, Infrared enhanced analytic coupling and chiral symmetry breaking in QCD. J. Phys. G **31**, 997 (2005). [arXiv:hep-ph/0504195](#)
125. K.A. Milton, I.L. Solovtsov, O.P. Solovtsova, Analytic perturbation theory and inclusive tau decay. Phys. Lett. B **415**, 104 (1997). [arXiv:hep-ph/9706409](#)
126. K.A. Milton, I.L. Solovtsov, O.P. Solovtsova, The Adler function for light quarks in analytic perturbation theory. Phys. Rev. D **64**, 016005 (2001). [arXiv:hep-ph/0102254](#)
127. B.A. Magradze, The gluon propagator in analytic perturbation theory. Conf. Proc. C **980518**, 158 (1999). [arXiv:hep-ph/9808247](#)
128. S. Peris, M. Perrottet, E. de Rafael, Matching long and short distances in large- N_c QCD. JHEP **9805**, 011 (1998). [arXiv:hep-ph/9805442](#)
129. B.A. Magradze, Testing the concept of quark-hadron duality with the ALEPH τ decay data. Few Body Syst. **48**, 143 (2010). [arXiv:1005.2674](#) [hep-ph] [Erratum: Few Body Syst. **53**, 365 (2012)]
130. B.A. Magradze, Strong coupling constant from τ decay within a dispersive approach to perturbative QCD. Proc. A. Razmadze Math. Inst. **160**, 91–111 (2012). [arXiv:1112.5958](#) [hep-ph]
131. A.V. Nesterenko, J. Papavassiliou, A novel integral representation for the Adler function. J. Phys. G **32**, 1025 (2006). [arXiv:hep-ph/0511215](#)
132. A.V. Nesterenko, Dispersive approach to QCD and inclusive tau lepton hadronic decay. Phys. Rev. D **88**, 056009 (2013). [arXiv:1306.4970](#) [hep-ph]
133. A.V. Nesterenko, Hadronic vacuum polarization function within dispersive approach to QCD. J. Phys. G **42**, 085004 (2015). [arXiv:1411.2554](#) [hep-ph]
134. A.V. Nesterenko, Electron-positron annihilation into hadrons at the higher-loop levels. Eur. Phys. J. C **77**, 844 (2017). [arXiv:1707.00668](#) [hep-ph]
135. A.V. Nesterenko, *Strong Interactions in Spacelike and Timelike Domains: Dispersive Approach* (Elsevier, Amsterdam, 2016). eBook ISBN:9780128034484
136. J. Blümlein, G. Falcioni, A. De Freitas, The complete $O(\alpha_s^2)$ non-singlet heavy flavor corrections to the structure functions $g_{1,2}^{ep}(x, Q^2)$, $F_{1,2,L}^{ep}(x, Q^2)$, $F_{1,2,3}^{p(v)}(x, Q^2)$ and the associated sum rules. Nucl. Phys. B **910**, 568 (2016). [arXiv:1605.05541](#) [hep-ph]